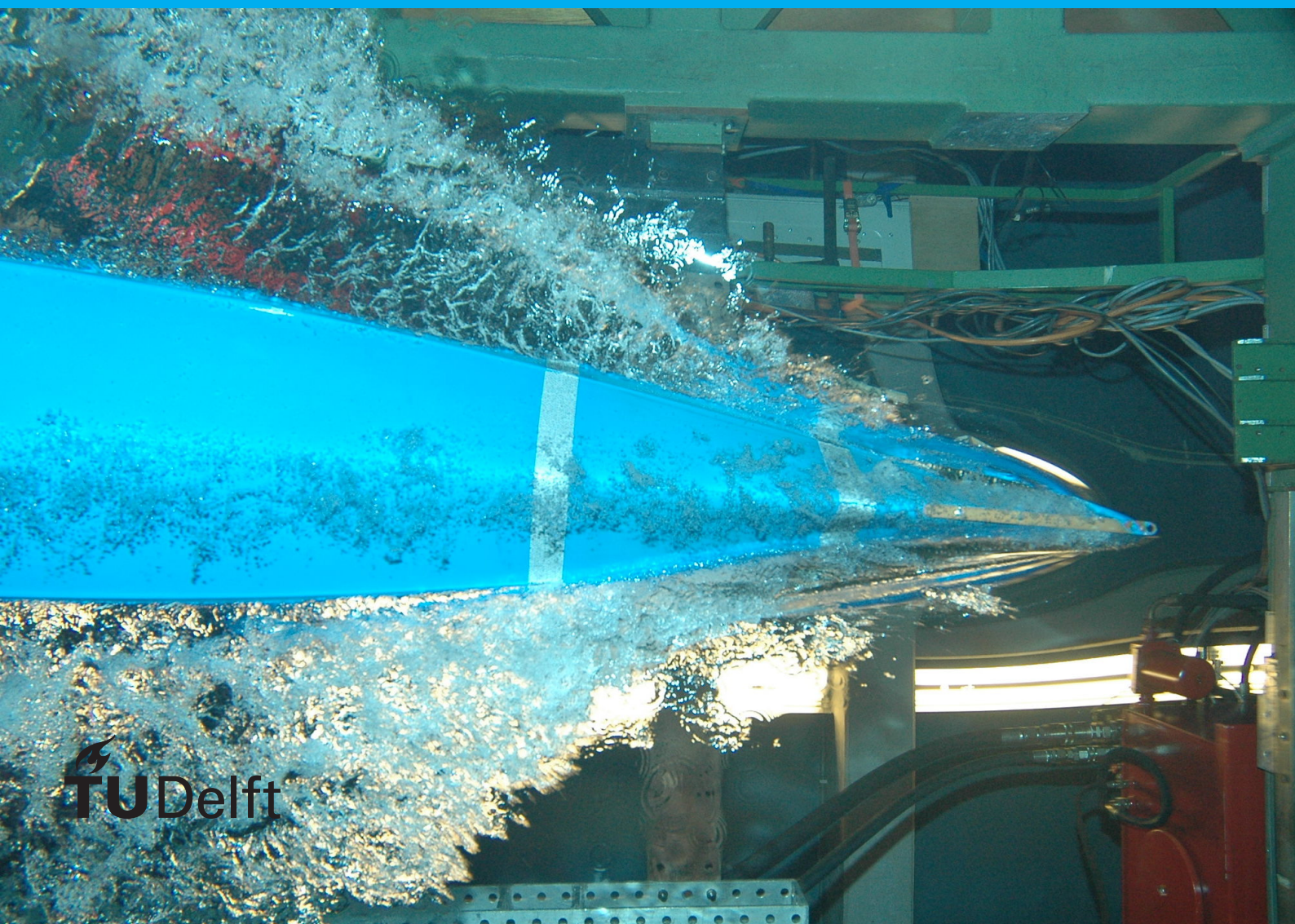# Analytical approach to hollow core Photonic Crystal Fiber for gas sensing

Lisanne Abutan

Analytical approach to hollow core Photonic Crystal Fiber for gas sensing

by

Lisanne Abutan

to obtain the degree of Bachelor of Science
at the Delft University of Technology

Student number:	4835506	
Project duration:	September 1, 2021 – August 29, 2022	
Thesis committee:	Dr. ir. A. J. L. Adam,	TU Delft, supervisor
	Dr. A. Heinlein,	TU Delft, supervisor
	Dr. ir. J. P. Hoogenboom,	TU Delft
	Dr. J. L. A. Dubbeldam,	TU Delft

TUDelft

Preface

Over the duration of my research I came across many challenges. I would like to thank my parents for supporting me throughout the whole process. Furthermore, I would like to thank my supervisors, Aurele Adam and Alexander Heinlein, but also Kristof Cools, who took on the role as my mathematics supervisor at the start. For the duration of this project, I have had many enlightening conversations with them, besides their great guidance and knowledgeable input. Then, I would like to thank Thomas Esselink, who assisted me with Comsol issues and supplied me with a working Comsol model. My project was a cooperation between the imaging physics department of the TU Delft and TNO. I would like to thank Man Xu from TNO for helping at the start of my project. Finaly, I would like to thank my friends for their uplifting words and for motivation me for during late night study sessions in the library.

<div align="right">

Lisanne Abutan
Delft, July 2022

</div>

Abstract

Interference of light can be used to determine the concentration of a gas, called gas sensing. The absorption of the light by the gas molecules is measured based on the phase change of the light. In this report, a hollow core photonic crystal fiber is treated. The gas sample is inserted into the hollow core. Photonic crystal fibers possess the characteristic to have electromagnetic modes confined to the core with low attenuation. This means that there can be a high interference rate between the gas and light, which is desirable for gas sensing.

First, less complicated optical fibers were studied. The analytical solution of the electric and magnetic field for the TE and TM modes of the simple fiber were derived and for the TE modes of the step-index fiber. These results were compared to simulation done with COMSOL Multiphysics. Photonic crystal fiber with circular core was then simulated with COMSOL Multiphysics, but the results did not match with the literature. Therefore another photonic crystal fiber was simulated with a star-shaped core. The simulation results found modes concentrated in the core, with low attenuation.

It was attempted to get similar results with a three layer step-index fiber, by varying the imaginary refractive index of the middle layer. The attenuation of the three layer fiber was much higher than that of the photonic crystal fiber for all simulations. This indicates that the three layer step-index fiber does not support propagation modes that are confined to the core. Further research could be done by studying the effect of the radius of the middle layer and the real part of the refractive index.

Contents

List of symbols

Symbol	Description	Unit
c	Speed of light	[m·s^{-1}]
$\mathbf{E}$	Electric field	[V·m^{-1}]
$\mathbf{E}_0$	Electric field independent of z and t	[Vm^{-1}]
E_r	Electric field in the r-direction	[V·m^{-1}]
E_θ	Electric field in the θ-direction	[V·m^{-1}]
E_x	Electric field in the x-direction	[V·m^{-1}]
E_y	Electric field in the y-direction	[V·m^{-1}]
E_z	Electric field in the z-direction	[V·m^{-1}]
$\mathbf{H}$	Magnetic field	[A·m^{-1}]
H_{0z}	Magnetic field component in the z-direction independent of z and t	[A·m^{-1}]
H_r	Electric field in the r-direction	[A·m^{-1}]
H_θ	Electric field in the θ-direction	[A·m^{-1}]
H_x	Magnetic field in the x-direction	[A·m^{-1}]
H_y	Magnetic field in the y-direction	[A·m^{-1}]
H_z	Magnetic field in the z-direction	[A·m^{-1}]
I_ν	Modified Bessel function of index ν	
J_ν	Bessel function of index ν	
K_ν	Macdonald function of index ν	
k_0	Wavenumber in vacuum	[m^{-1}]
k_c	Variable expression $\sqrt{n^2\omega^2/c^2}$	[m^{-1}]
k_{c1}	Variable expression $\sqrt{k_0^2 n_1^2 - k_z^2}$	[m^{-1}]
k_{c2}	Variable expression $\sqrt{k_z^2 - k_0^2 n_2^2}$	[m^{-1}]
k_z	Wavenumber in propagation direction z	[m^{-1}]
n	Refractive index	[-]
n_1	Refractive index of medium 1	[-]
n_2	Refractive index of medium 2	[-]
r	Radial coordinate	[m]
t	Time	[s]
x	Coordinate in the x-direction	[m]
x'	Variable expression $k_c r$	[-]
x_1	Variable expression $k_{c1} r$	[-]
x_2	Variable expression $k_{c2} r$	[-]
y	Coordinate in the y-direction	[m]
Y_ν	Bessel function of the second kind of index ν	
z	Coordinate of the direction of propagation	[m]
ε	Permittivity	[s^4·A^2·kg^{-1}·m^{-3}]
ε_1	Permittivity of medium 1	[s^4·A^2·kg^{-1}·m^{-3}]
ε_2	Permittivity of medium 2	[s^4·A^2·kg^{-1}·m^{-3}]
μ	Magnetic permeability	[kg·m·s^{-2}·A^{-2}]
μ_0	Magnetic permeability in vacuum	[kg·m·s^{-2}·A^{-2}]
ω	Angular frequency	[s^{-1}]
θ	Azimuth angle	[-]

1

Introduction

Currently, there is a quickly growing need for sustainable energy. As fossil fuel is limited and has a negative influence on the climate, the fossil fuel should be replaced by renewable energy. In the European Climate Law it is stated that the EU should be climate neutral by 2050.[29] Hydrogen can help in this process, but it also brings some challenges. When hydrogen is used as energy source, it does not produce any greenhouse gasses and the supply is unlimited, as it can be made from water. However, to make hydrogen, energy is needed. To be entirely climate neutral, the hydrogen should be made with sustainable energy sources. In that case, the hydrogen is called "green hydrogen".[8]
The main disadvantage of hydrogen is that it is highly flammable.[22] When it comes in contact with oxygen, it is very explosive. Therefore, it is important for the use, transport and storage of hydrogen, that the oxygen percentage is below a certain threshold. When there is a leak in a hydrogen storage tank or during transport, this has to be noticed quickly. To achieve this, instruments are needed that can accurately measure the concentration of hydrogen in a gas mixture. Optical fibers are often used for this. In 1978, E. Yablonovitch[33] and S. John[17] were the first to write about the photonic band gap.[1] This started the research into photonic crystal fibers and their use as gas sensing instrument.

This report will explain the necessary theory about gas sensing and photonic crystal fibers in Chapter 2. Chapter 3 contains an analytical derivation of the electric and magnetic field for a simple fiber and a step-index fiber. Chapter 4 is the Experimental Setup, in which the basics of COMSOL Multiphysics[6] are explained and the settings for the various simulations that are computed. In Chapter 5 the results are presented and discussed. Chapter 6 contains the Conclusion.

2

Theory

2.1. Fiber sensing for gas detection

To measure the concentration of a certain element in a gas mixture, optical fibers can be used. Gas molecules can absorb light for specific wavelengths, depending on the kind of gas.[13] This can be used to determine the concentration or presence of a gas in a sample. This is called spectroscopy. Another way to determine the gas concentration in a sample is based on interference. The concentration of gas in a medium determines the refractive index, which affects the speed of light through that medium. Therefore, the phase shift of the light contains information about the gas concentration. Optical fiber can be used for this, because they can guide light through the core with low loss.[21]

Classical optical fibers guide modes based on internal reflections. The modes in a hollow core photonic crystal fiber are the result of a photonic bandgap. In a hollow core photonic crystal fiber the interaction of the light with the gas is higher. The loss of light confined in the core is lower than for optical fibers based on total internal reflection.[31] This gives the photonic crystal fiber a higher sensitivity,[16] but it also offers a much longer interaction length.[27] This makes it is much more accurate on shorter distances as well, compared to classical optical fibers.

The principle of a hollow core photonic crystal fiber is the following. The gas sample is pumped into the hollow core. A light beam with adjustable wavelength is guided into the core from one side. This will be called the pump light beam, as seen in Figure 2.1. When this light has the 'right' wavelength, it will excite the molecules in the gas. For what wavelength this happens depends on the kind of molecules. After the molecules are excited, they return to the ground state. This generates heat, which causes changes in the temperature, density, pressure and refractive index of the fiber. The dimensions of the fiber can also change due to the heat. From the other side, another light beam is sent into the core of the fiber, but this one has a different wavelength. Called the probe light beam. Due to the heat from the excited molecules, the phase of the probe light beam changes. This change thus contains information about the amount of heating. With the knowledge of the used pump wavelength, the percentage of different kind of molecules can be determined. In this process, the structure and the refractive index of the fiber play an important role.
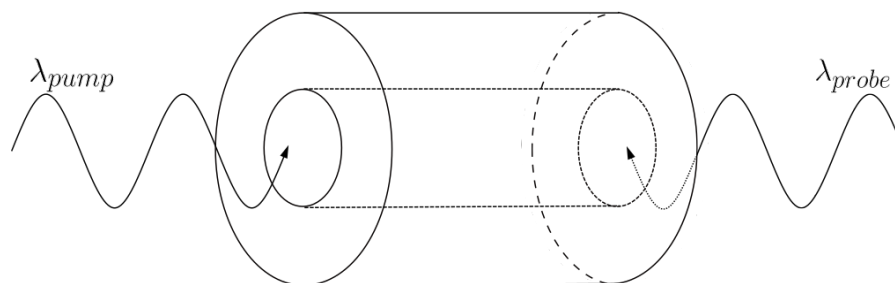

Figure 2.1: Schematic drawing of the use of the photonic crystal fiber. The incoming pump light beam with adjustable wavelength λ_{pump} and probe light beam with wavelength λ_{probe}.

2.2. Photonic crystal fiber

The cladding of a photonic crystal fiber (PCF) consists of holes in a certain periodic structure. For this report a honeycomb structured fiber is used, specifically from the fiber HC-1550-02 (Thorlabs).[12] This fiber was chosen based on an article from Wan et al.[31] A cross section of the fiber can be seen in Figure 2.2.

This air hole structure creates bandgaps: wavelengths that lie inside this bandgap cannot travel through the cladding and are therefore locked in the core of the fiber.[1] This is also the reason that the interaction of light with gas in the core can be very high for photonic crystal fibers, which is desirable for gas sensing.[27]

To be able to calculate the electric and magnetic field inside the fiber more quickly, it could be helpful to simplify the honeycomb structure. In this report it is investigated whether the region with the holes, surrounding the core, can be simplified to a medium with one refractive index. This will simplify the photonic crystal fiber to a step index fiber with three layers. For the three layer step-index fiber, simulations to calculate the electric and magnetic field can be done much quicker or even analytically.
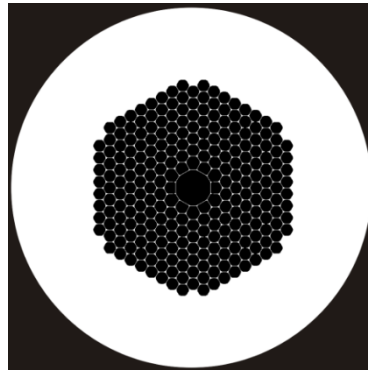

Figure 2.2: Cross section of the HC-1550-02 photonic crystal fiber.[28]

2.3. Simplification Photonic Crystal Fiber

In this report the main focus is to simplify the geometry of the photonic crystal fiber, as shown in Figure 2.2, to a step-index fiber with 3 layers. The step index fiber that is used for the simplification is shown in Figure 2.3. The effective refractive index n_{eff} can be adjusted, to best resemble the photonic crystal bandgap fiber. The values for n_1, n_3, R_1, R_2 and R_3 are predetermined.
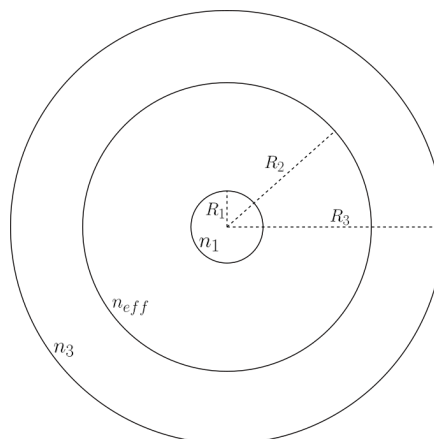

Figure 2.3: Step index fiber with three layers, that is used to simplify the photonic crystal fiber. With radii R_1, R_2 and R_3 and refractive indexes n_1, n_{eff} and n_3.

3

Fibers

To gain some knowledge about modes inside a fiber two basic fibers are investigated, the simple fiber and the step-index fiber. The modes in the fibers are calculated analytically in this chapter. Starting with the simple fiber and then moving onto the step-index fiber. This is a fiber with two layers with different refractive indexes. The field inside a fiber can be derived analytically by working out the Maxwell equations and applying the right boundary conditions.

3.1. Maxwell Equations

The electric and magnetic field in a waveguide adhere to the Maxwell equations without currents or charges, given in equation (3.1)-(3.4). [7]

$$\nabla \cdot \mathbf{E} = 0 \tag{3.1}$$

$$\nabla \times \mathbf{E} = -\mu \frac{\partial \mathbf{H}}{\partial t} \tag{3.2}$$

$$\nabla \cdot \mathbf{H} = 0 \tag{3.3}$$

$$\nabla \times \mathbf{H} = \varepsilon \frac{\partial \mathbf{E}}{\partial t} \tag{3.4}$$

with $\mathbf{E}$ the electric field, $\mathbf{H}$ the magnetic field, μ the permeability and ε the permittivity.

For the rest of this report, we consider waveguides with modes propagating in the z-direction. Then the following ansatz is used for the electric and magnetic field.[20]

$$\mathbf{E} = \mathbf{E}_0 e^{i(\omega t - k_z z)} \tag{3.5}$$

$$\mathbf{H} = \mathbf{H}_0 e^{i(\omega t - k_z z)} \tag{3.6}$$

with ω the angular frequency and k_z the wavenumber in the direction of propagation, also known as the propagation constant.

Equations (3.5) and (3.6) can be inserted into equations (3.2) and (3.4). This gives the following set of equations:

$$\begin{cases} \dfrac{\partial E_z}{\partial y} + ik_z E_y = -i\omega\mu H_x \\[2mm] -ik_z E_x - \dfrac{\partial E_z}{\partial x} = -i\omega\mu H_y \\[2mm] \dfrac{\partial E_y}{\partial x} - \dfrac{\partial E_x}{\partial y} = -i\omega\mu H_z \\[2mm] \dfrac{\partial H_z}{\partial y} + ik_z H_y = i\omega\varepsilon E_x \\[2mm] -ik_z H_x - \dfrac{\partial H_z}{\partial x} = i\omega\varepsilon E_y \\[2mm] \dfrac{\partial H_y}{\partial x} - \dfrac{\partial H_x}{\partial y} = i\omega\varepsilon E_z \end{cases} \tag{3.7}$$

7

Equation (3.7) can also be derived for cylindrical coordinates, with r the radial coordinate, θ the azimuth angle and z the axial coordinate. It is more useful for the circular fibers that are considered, to use cylindrical coordinates. This can be done using the equation for the curl in cylindrical coordinates (equation (3.7)).[9]

$$\nabla \times \mathbf{u} = \left(\frac{1}{r} \frac{\partial u_z}{\partial \theta} - \frac{\partial u_\theta}{\partial z} \right) \cdot \hat{\mathbf{r}} + \left(\frac{\partial u_r}{\partial z} - \frac{\partial u_z}{\partial r} \right) \cdot \hat{\boldsymbol{\theta}} + \frac{1}{r} \left(\frac{\partial (r u_\theta)}{\partial r} - \frac{\partial u_r}{\partial \theta} \right) \cdot \hat{\mathbf{z}} \qquad (3.8)$$

Now working out equations (3.2) and (3.4) give the following cylindrical set of equations, that can be found in equation (3.9). [26]

$$\begin{cases} \dfrac{1}{r} \dfrac{\partial E_z}{\partial \theta} + i k_z E_\theta = -i\omega\mu H_r \\[2mm] -i k_z E_r - \dfrac{\partial E_z}{\partial r} = -i\omega\mu H_\theta \\[2mm] \dfrac{1}{r} \dfrac{\partial (r E_\theta)}{\partial r} - \dfrac{1}{r} \dfrac{\partial E_r}{\partial \theta} = -i\omega\mu H_z \\[2mm] \dfrac{1}{r} \dfrac{\partial H_z}{\partial \theta} + i k_z H_\theta = i\omega\varepsilon E_r \\[2mm] -i k_z H_r - \dfrac{\partial H_z}{\partial r} = i\omega\varepsilon E_\theta \\[2mm] \dfrac{1}{r} \dfrac{\partial (r H_\theta)}{\partial r} - \dfrac{1}{r} \dfrac{\partial H_r}{\partial \theta} = i\omega\varepsilon E_z \end{cases} \qquad (3.9)$$

From this the transverse electric field components can be simplified to equations (3.10) and (3.11)

$$E_r = \frac{i}{(k_z^2 - \omega^2 \varepsilon \mu)} \left(\frac{\omega\mu}{r} \frac{\partial H_z}{\partial \theta} + k_z \frac{\partial E_z}{\partial r} \right) \qquad (3.10)$$

$$E_\theta = \frac{-i}{(k_z^2 - \omega^2 \varepsilon \mu)} \left(\omega\mu \frac{\partial H_z}{\partial r} - \frac{k_z}{r} \frac{\partial E_z}{\partial \theta} \right) \qquad (3.11)$$

The transverse magnetic field components can be written as (3.12) and (3.13).

$$H_r = \frac{i}{(k_z^2 - \omega^2 \varepsilon \mu)} \left(k_z \frac{\partial H_z}{\partial r} - \frac{\omega\varepsilon}{r} \frac{\partial E_z}{\partial \theta} \right) \qquad (3.12)$$

$$H_\theta = \frac{i}{(k_z^2 - \omega^2 \varepsilon \mu)} \left(\frac{k_z}{r} \frac{\partial H_z}{\partial \theta} + \omega\varepsilon \frac{\partial E_z}{\partial r} \right) \qquad (3.13)$$

The modes in a fiber can be transverse electromagnetic modes (TEM modes), transverse electric modes (TE modes), transverse magnetic modes (TM modes) or hybrid modes. The electric and magnetic field components of TEM modes lie only in the transverse plane and there is no field in the direction of propagation. TE modes have an electric field that is completely in the transverse direction, so there is no electric field along the direction of propagation. The TM modes do not have a magnetic field in the direction of propagation, but only in the transverse direction. Hybrid modes can have both an electric and magnetic field component in the direction of propagation.

Figure 3.1 shows how TE and TM modes are created by total internal reflection inside a fiber. For the TE mode, the E field is completely transverse and has no component in the z-direction. Conversely, the magnetic field is completely in the transverse direction for the TM mode and has no component in the direction of propagation.

For the simple fiber, the analytical solution of the TE and TM modes will be derived and for the step-index fiber, only the TE-modes, as the TM modes can be derived in a similar manner. For the TE mode, the electric field in the propagation direction is $E_z = 0$, resulting in the following simplification of equations (3.10), (3.11), (3.12) and (3.13).

$$E_r = \frac{i\omega\mu}{(k_z^2 - \omega^2 \varepsilon \mu) r} \frac{\partial H_z}{\partial \theta} \qquad (3.14)$$

(a) The field directions for a TE mode.
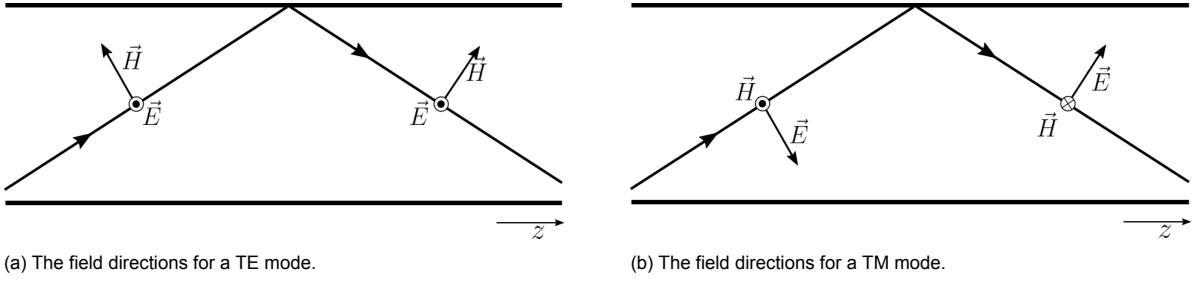
(b) The field directions for a TM mode.

Figure 3.1: The electric and magnetic field components before and after reflection at a boundary.

$$E_\theta = \frac{-i\omega\mu}{(k_z^2 - \omega^2\varepsilon\mu)} \frac{\partial H_z}{\partial r} \tag{3.15}$$

$$H_r = \frac{ik_z}{(k_z^2 - \omega^2\varepsilon\mu)} \frac{\partial H_z}{\partial r} \tag{3.16}$$

$$H_\theta = \frac{ik_z}{(k_z^2 - \omega^2\varepsilon\mu)\, r} \frac{\partial H_z}{\partial \theta} \tag{3.17}$$

For the TM mode, $H_z = 0$, resulting in this simplification.

$$E_r = \frac{ik_z}{(k_z^2 - \omega^2\varepsilon\mu)} \frac{\partial E_z}{\partial r} \tag{3.18}$$

$$E_\theta = \frac{ik_z}{(k_z^2 - \omega^2\varepsilon\mu)\, r} \frac{\partial E_z}{\partial \theta} \tag{3.19}$$

$$H_r = \frac{-i\omega\varepsilon}{(k_z^2 - \omega^2\varepsilon\mu)\, r} \frac{\partial E_z}{\partial \theta} \tag{3.20}$$

$$H_\theta = \frac{i\omega\varepsilon}{(k_z^2 - \omega^2\varepsilon\mu)} \frac{\partial E_z}{\partial r} \tag{3.21}$$

Besides the Maxwell equations, the electric field $\mathbf{E}$ and magnetic field $\mathbf{H}$ also need to satisfy the wave equation, given in equation (3.22).[5]

$$\nabla^2 \mathbf{u} = \varepsilon\mu \frac{\partial^2 \mathbf{u}}{\partial t^2} = \frac{n^2}{c^2} \frac{\partial^2 \mathbf{u}}{\partial t^2} \tag{3.22}$$

Here $\mathbf{u}$ is some function that should adhere to the wave equation, in our case $\mathbf{E}$ and $\mathbf{H}$. n is the refractive index of the medium through which the wave propagates and c is the speed of light.

3.2. Simple Fiber

The fiber that we consider in this section is the simple fiber with perfect conductor boundary conditions. In figure 3.2, the cross section of a simple fiber is shown, with the radius R and refractive index n.

3.2.1. Analytical solution TE-modes

To calculate the field inside the fiber, the Maxwell equations from the previous section need to be solved. The steps that are taken in this calculation are based on "Lectures on Theory of Microwave and Optical Waveguides"[3], "Fundamentals of Optical Waveguides"[26], "Microwave and Optical Waveguides"[7], "Cavity basics"[15] and "Applications of Maxwell's equations"[5]. Equation (3.6) in the z-direction is

$$H_z(r, \theta, z) = H_{0z}(r, \theta)e^{i(\omega t - k_z z)} \tag{3.23}$$

where H_{0z} can depend on r and θ. This, in combination with the wave equation (3.22), gives the following partial differential equation for H_{0z}.

$$\frac{1}{r}\frac{\partial}{\partial r}\left(r\frac{\partial H_{0z}}{\partial r}\right) + \frac{1}{r^2}\frac{\partial^2 H_{0z}}{\partial \theta^2} + H_{0z}\left(\frac{n^2\omega^2}{c^2} - k_z^2\right) = 0 \tag{3.24}$$
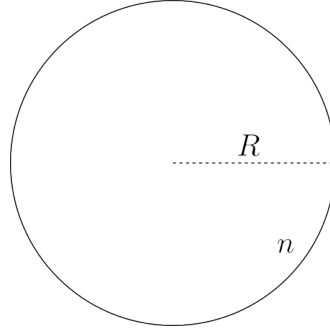
Figure 3.2: Schematic sketch of the cross section of the simple fiber, with R the radius of the fiber ,n the refractive index and perfect conductor boundary conditions.

To solve this equation we use separation of variables. Assume that H_{0z} can be written as a multiplication of a function of r and a function of θ.

$$H_{0z}(r,\theta) = F(r)\Theta(\theta) \tag{3.25}$$

Inserting equation (3.25) into equation (3.24), this gives:[5]

$$\frac{r}{F(r)}\frac{\partial}{\partial r}\left(r\frac{\partial}{\partial r}F(r)\right) + r^2\left(\frac{n^2\omega^2}{c^2} - k_z^2\right) = -\frac{1}{\Theta(\theta)}\frac{\partial^2\Theta(\theta)}{\partial\theta^2} = m^2 \tag{3.26}$$

where m is the separation constant. For $\Theta(\theta)$ the solution is

$$\Theta(\theta) = a\cos(m\theta) + b\sin(m\theta) \tag{3.27}$$

where a and b are constants. The fiber has cylindrical symmetry, which means that it can be mirrored over a radial axis. Choose the axis $y = 0$, giving $\Theta(\theta) = \Theta(-\theta)$. Using equation (3.27), this reduces to $a\cos(m\theta) + b\sin(m\theta) = a\cos(-m\theta) + b\sin(-m\theta)$.
From this it follows that $b = 0$. For $F(r)$ the equation reduces to

$$r\frac{\partial}{\partial r}\left(r\frac{\partial}{\partial r}F(r)\right) + F(r)\left(r^2\left(\frac{n^2\omega^2}{c^2} - k_z^2\right) - m^2\right) = 0 \tag{3.28}$$

Let $k_c^2 = \frac{n^2\omega^2}{c^2} - k_z^2$ and then introduce the change of variable $x' = k_c r$. Equation (3.28) can then be written as

$$x'\frac{\partial}{\partial x'}\left(x'\frac{\partial}{\partial x}F(x')\right) + F(x')\left(x'^2 - m^2\right) = 0 \tag{3.29}$$

This can be written as

$$x'^2\frac{\partial^2 F(x')}{\partial x'^2} + x'\frac{\partial F(x')}{\partial x'} + F(x')\left(x'^2 - m^2\right) = 0 \tag{3.30}$$

This is written in a standard form, for which the solution is a Bessel function.
The Bessel function is the solution of the Bessel equation, which is a differential equation that is often the result of separation of variables with cylindrical coordinates. The Bessel equation of index ν is:

$$x^2\frac{d^2u}{dx^2} + x\frac{du}{dx} + (x^2 - \nu^2)u = 0 \tag{3.31}$$

with u a function depending on some variable called x. The solution is given by

$$u(x) = B_1 J_\nu(x) + B_2 Y_\nu(x) \tag{3.32}$$

J_ν is the Bessel function of the first kind of index ν and Y_ν is the Bessel function of the second kind of index ν, also called the Neumann function.[19] The first four Bessel functions of the first kind are plotted in Figure 3.3 and the first four Bessel functions of the second kind in Figure 3.4. The plots are made with Python.[14]
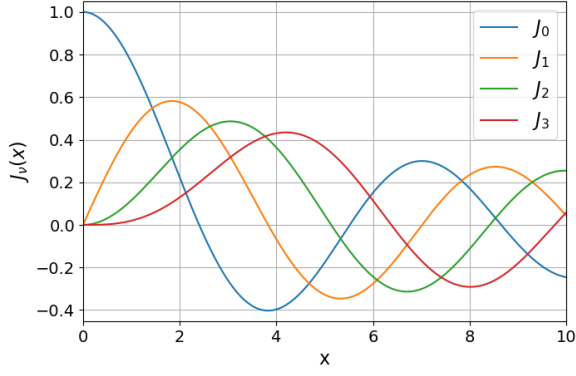
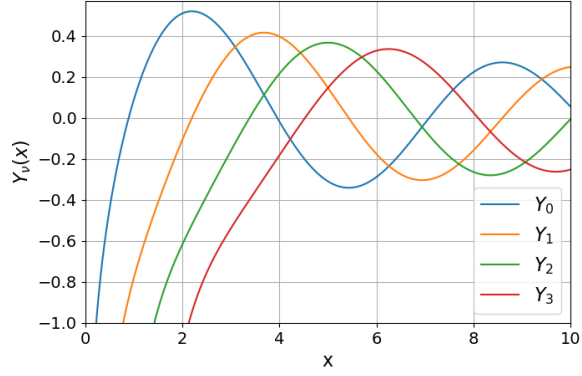Figure 3.3: The first four Bessel functions of the first kind J_ν.

Figure 3.4: The first four Bessel functions of the second kind Y_ν.

For equation (3.30), the general solution is then given by equation (3.32) with index m.

$$F(x') = B_1 J_m(x') + B_2 Y_m(x') \tag{3.33}$$

with B_1 and B_2 constants. The second order Bessel function, $Y_m(r)$, goes to infinity at $r = 0$, as can be seen in Figure 3.4. The solution needs to be finite at $r = 0$. Therefore, $B_2 = 0$. Inserting equations (3.27) and (3.33) into equation (3.25) and then (3.23) gives the following z-component of the magnetic field.

$$H_z(r, \theta, z) = H_1 J_m(k_c r) \cos(m\theta) e^{i(\omega t - k_z z)} \tag{3.34}$$

where H_1 is a constant. With equations (3.14) and (3.15) the transverse components of the electric field can be calculated. Then use the expression of $k_c^2 = \frac{n^2 \omega^2}{c^2} - k_z^2$ again and keep in mind that $\frac{c}{n} = \frac{1}{\sqrt{\varepsilon \mu}}$.

$$E_r(r, \theta, z) = -H_1 \frac{i\omega\mu m}{k_c^2 r} J_m(k_c r) \sin(m\theta) e^{i(\omega t - k_z z)} \tag{3.35}$$

$$E_\theta(r, \theta, z) = -H_1 \frac{i\omega\mu}{k_c} J'_m(k_c r) \cos(m\theta) e^{i(\omega t - k_z z)} \tag{3.36}$$

The perfect conductor boundary condition implies that the electric field transverse to the boundary is zero.[11] This means that $E_\theta = 0$ and $E_z = 0$ at $r = R$, so the electric field has to be entirely in the radial direction. The magnetic field is perpendicular to the electric field. Therefore, this should be zero in the radial direction ($H_r(R, \theta, z) = 0$). From equation (3.9) and (3.36) it can be seen that

$$H_r(r, \theta, z) = -\frac{k_z}{\omega\mu} E_\theta(r, \theta, z) = H_1 \frac{ik_z}{k_c} J'_m(k_c r) \cos(m\theta) e^{i(\omega t - k_z z)} \tag{3.37}$$

To satisfy the boundary condition, the following should hold.

$$J'_m(k_c R) = 0 \tag{3.38}$$

From this k_c can be calculated. As can be seen in Figure 3.3, J_ν has multiple maxima and minima. This means that there are multiple values for k_c for which equation (3.38) holds. The n'th zero of the derivative of the m'th Bessel function J_m gives the value for the TE$_{mn}$ mode. With this the absolute value of the electric field for the TE-modes can be calculated.

3.2.2. Analytical solution TM-modes
The derivation of the TM-modes is similar to that of the TE-modes. The electric field in the z-direction has to satisfy the wave equation (3.22). Similar to the magnetic field for the TE-modes, the electric field in the longitudinal direction can be written as

$$E_z(r, \theta, z) = E_{0z}(r, \theta) e^{i(\omega t - k_z z)} \tag{3.39}$$

also with the condition that E_{0z} should be finite at $r = 0$. In the same way as for the magnetic field for the TE-modes (equation (3.34)), with the wave equation (3.22), the electric field along the z-direction is given by

$$E_z(r, \theta, z) = E_1 J_m(k_c r) \cos(m\theta) e^{i(\omega t - k_z z)}. \tag{3.40}$$

Using equations (3.18) and (3.19), the transverse electric field components can be derived.

$$E_r(r, \theta, z) = -E_1 \frac{ik_z}{k_c} J_m'(k_c r) \cos(m\theta) e^{i(\omega t - k_z z)} \tag{3.41}$$

$$E_\theta(r, \theta, z) = E_1 \frac{ik_z m}{k_c^2 r} J_m(k_c r) \sin(m\theta) e^{i(\omega t - k_z z)} \tag{3.42}$$

The same as with the TE-modes, the magnetic field in the radial direction should be zero at the boundaries $r = R$. Equation (3.20) gives

$$H_r(r, \theta, z) = -E_1 \frac{im\omega\varepsilon}{k_c^2 r} J_m(k_c r) \sin(m\theta) e^{i(\omega t - k_z z)} \tag{3.43}$$

This results in the following condition that has to be satisfied.

$$J_m(k_c R) = 0 \tag{3.44}$$

Similar as before, Figure 3.3 shows that the Bessel functions of first kind have multiple intersections with the x-axis, so multiple zeros. This means again that there are multiple values for k_c for which equation (3.44) hold. The n'th zero of the m'th Bessel function J_m corresponds to the TM$_{mn}$ mode. With equation (3.41) and (3.42) the electric field of the TM$_{mn}$-mode can then be calculated.

In Chapter 4.2 the simple fiber is simulated in COMSOL Multiphysics. In Chapter 5.1.1 the analytical solutions for both the TE and TM modes are calculated for the simple fiber and compared to the COMSOL simulation.

3.3. Step-Index Fiber

In this section the step-index fiber is analysed. The derivation of the equations is based on "An Introduction to Optical Fibers"[2], "Fundamentals of Optical Waveguides"[26] and "Estimation of photonic band gap in the hollow core cylindrical multilayer structure"[4]. A cross section of the fiber is shown schematically in figure 3.5.
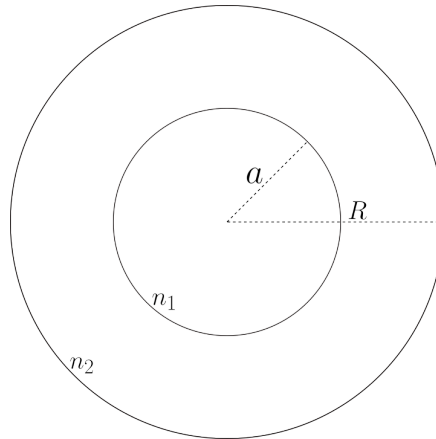

Figure 3.5: Schematic sketch of a cross section of the step-index fiber, with R the radius of the fiber and a the inner radius, with n_1 the refractive index for $0 \leq r \leq a$ and n_2 the refractive index for $r > a$, where r is the radial coordinate. Conductor boundary conditions apply at $r = R$.

3.3.1. Analytical solution

In the same way as for the simple fiber, the step-index fiber is analysed. First, the magnetic field in z-direction (equation (3.23)) is inserted into the wave equation (3.22). The magnetic field in the z-direction can be separated in a part that depends on θ and another part that depends on r (see equation (3.25)). This leads to the solution for the θ dependent part given by equation (3.27), same as for the simple fiber, because this part does not depend on the radius or any material properties. The r dependent solution, and thus also the total solution, will be different for $r < a$ and $r > a$, as the refractive index n is different and, therefore, also ω. This gives the following for the magnetic field.

$$H_{0z}(r,\theta) = \begin{cases} F_1(r)\cos(m\theta) & 0 \le r \le a \\ F_2(r)\cos(m\theta) & r > a \end{cases} \tag{3.45}$$

Then the boundary condition is used that the electric field tangential to the interface should be continuous and the magnetic field perpendicular to the interface should be continuous. [26][20] This means that $H_{0z}(a_-,\theta) = H_{0z}(a_+,\theta)$ and $H_\theta(a_-,\theta,z) = H_\theta(a_+,\theta,z)$, where a_- and a_+ mean that this should be evaluated at $r = a$ from below and above, respectively. Using equations (3.17) to get $H_\theta(r,\theta,z)$ this implies the following.

$$F_1(a) = F_2(a) \tag{3.46}$$

$$\frac{ik_z}{(k_z^2 - \omega^2\varepsilon_1\mu)\,a}F_1(a)m\sin(m\theta) = \frac{ik_z}{(k_z^2 - \omega^2\varepsilon_2\mu)\,a}F_2(a)m\sin(m\theta) \tag{3.47}$$

Where $\omega^2\varepsilon_1\mu = k_0^2 n_1^2$ for the core and $\omega^2\varepsilon_2\mu = k_0^2 n_2^2$ for the cladding. The magnetic permeability for $r \le a$ and $r > a$ is taken to be the same. There are no significant magnetic effects at optical frequencies, therefore the magnetic permeability can be taken as a constant $\mu = \mu_0$, the magnetic permeability in vacuum.[18] Equations (3.46) and (3.47) can only hold for all θ if $m = 0$. Which means that $\frac{\partial H_z}{\partial \theta} = 0$. Equations (3.14)-(3.17) then simplify to

$$E_r = H_\theta = 0 \tag{3.48}$$

$$E_\theta = \frac{-i\omega\mu}{\left(k_z^2 - k_0^2 n^2(r)\right)}\frac{\partial H_z}{\partial r} \tag{3.49}$$

$$H_r = \frac{ik_z}{\left(k_z^2 - k_0^2 n^2(r)\right)}\frac{\partial H_z}{\partial r} \tag{3.50}$$

Equation (3.26) remains the same, but with $m = 0$. For $H_{0z}(r,\theta)$ the θ dependent part $\Theta(\theta)$ becomes a constant (equation (3.27)). For the r dependent part, $F(r)$, there are two solutions, F_1 for $0 \le r \le a$ and F_2 for $r > a$. Using $\frac{\omega}{c} = k_0$, equation (3.28) becomes

$$\frac{\partial^2 F(r)}{\partial r^2} + \frac{1}{r}\frac{\partial F(r)}{\partial r} + F(r)\left(k_0^2 n^2(r) - k_z^2\right) = 0. \tag{3.51}$$

Now let $k_{c1}^2 = k_0^2 n_1^2 - k_z^2$ and $k_{c2}^2 = k_z^2 - k_0^2 n_2^2$. For the field inside the core, this results in equation (3.52) and for the cladding equation (3.53).

$$\frac{\partial^2 F_1(r)}{\partial r^2} + \frac{1}{r}\frac{\partial F_1(r)}{\partial r} + F_1(r)k_{c1}^2 = 0 \tag{3.52}$$

$$\frac{\partial^2 F_2(r)}{\partial r^2} + \frac{1}{r}\frac{\partial F_2(r)}{\partial r} - F_2(r)k_{c2}^2 = 0 \tag{3.53}$$

Introducing $x_1 = k_{c1}r$ and $x_2 = k_{c2}r$ equations (3.52) and (3.53) become

$$x_1^2\frac{\partial^2 F_1(x_1)}{\partial x_1^2} + x_1\frac{\partial F_1(x_1)}{\partial x_2} + F_1(x_1)x_1^2 = 0 \tag{3.54}$$

$$x_2^2\frac{\partial^2 F_2(x_2)}{\partial x_2^2} + x_2\frac{\partial F_2(x_2)}{\partial x_2} - F_2(x_2)x_2^2 = 0 \tag{3.55}$$

The equation for F_1 is the standard Bessel differential equation, from equation (3.31) with index 0. The solution has the following form [19]

$$F_1(x_1) = B_1 J_0(x_1) + B_2 Y_0(x_1) \tag{3.56}$$

At $r = 0$ the field should be finite, therefore $B_2 = 0$.

The equation for F_2 is not in the standard Bessel equation form.[19] This is the Bessel equation with complex argument $x = yi$, with y some real variable. When x in equation (3.31) is replaced with yi, this gives

$$y^2 \frac{d^2 u}{dy^2} + y \frac{du}{dy} - (y^2 + v^2)u = 0 \tag{3.57}$$

The solution to this equation is

$$u(y) = B_3 I_v(y) + B_4 K_v(y) \tag{3.58}$$

Here I_v is the modified Bessel function of index v and K_v is called the Macdonald function of index v. Figure 3.6 and Figure 3.7 are plots of the first four modified Bessel functions and Macdonald functions, respectively. The plots are made in Python.[14]
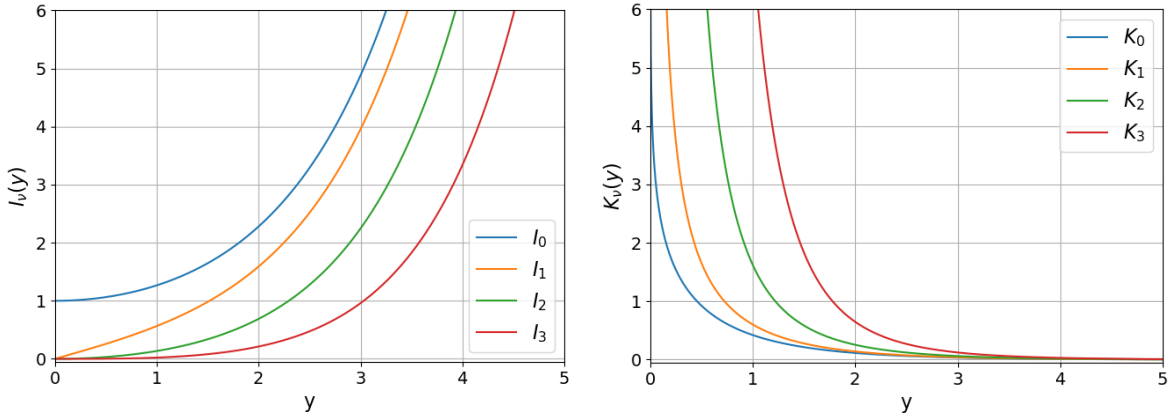

Figure 3.6: The first four modified Bessel functions I_v.   Figure 3.7: The first four Macdonald functions K_v.

The solutions for F_2 are thus the modified Bessel functions with index 0.

$$F_2(x_2) = B_3 I_0(x_2) + B_4 K_0(x_2) \tag{3.59}$$

The modified Bessel function of index 0 ($I_0(r)$) diverges to infinity at $r = \infty$, see Figure 3.6. The field should be bounded at infinity, therefore $B_3 = 0$. The total magnetic field in the z-direction from equation (3.45) is now given by

$$H_{z0}(r, \theta) = \begin{cases} B_1 J_0(k_{c1} r) & 0 \leq r \leq a \\ B_4 K_0(k_{c2} r) & r > a \end{cases} \tag{3.60}$$

The total electric and magnetic field tangential to the boundary at the interface $r = a$ should be continuous.[18] This includes E_θ, E_z, H_θ and H_z. As this is a TE mode, $E_z = 0$ and from equation (3.48), $H_\theta = 0$. With E_θ from equation (3.49), the following conditions apply at the interface.

$$B_1 J_0(k_{c1} a) = B_4 K_0(k_{c2} a) \tag{3.61}$$

$$\frac{B_1}{k_{c1}} J_0'(k_{c1} a) = -\frac{B_4}{k_{c2}} K_0'(k_{c2} a) \tag{3.62}$$

Solving for B_1 gives $B_1 = \frac{B_4 K_0(k_{c2} a)}{J_0(k_{c1} a)}$, so the two conditions together can be rewritten as

$$\frac{J_0'(k_{c1} a)}{k_{c1} J_0(k_{c1} a)} = -\frac{K_0'(k_{c2} a)}{k_{c2} K_0(k_{c2} a)} \tag{3.63}$$

Using the variables $\kappa_1 = k_{c1}a$ and $\kappa_2 = k_{c2}a$ and the expressions for the derivatives of Bessel functions $J_0'(x) = -J_1(x)$ and $K_0'(x) = -K_1(x)$,[19] the following is obtained.

$$\frac{J_1(\kappa_1)}{\kappa_1 J_0(\kappa_1)} = -\frac{K_1(\kappa_2)}{\kappa_2 K_0(\kappa_2)} \tag{3.64}$$

Beside this, there is another relation between κ_1 and κ_2, because $k_{c1}^2 - k_{c2}^2 = k_0^2 n_1^2 + k_0^2 n_2^2$.

$$\kappa_1^2 - \kappa_2^2 = k_0^2 a^2 \left(n_1^2 + n_2^2 \right) \tag{3.65}$$

With equation (3.64) and (3.65) the values of κ_1 and κ_2 can be calculated and then also k_{c1} and k_{c2}. The magnetic field in the z direction is then given by

$$H_z(r,\theta,z) = \begin{cases} B_1 J_0(k_{c1}r) e^{i(\omega t - k_z z)} & 0 \leq r \leq a \\ B_1 \frac{J_0(k_{c1}a)}{K_0(k_{c2}a)} K_0(k_{c2}r) e^{i(\omega t - k_z z)} & r > a \end{cases} \tag{3.66}$$

Then with equation (3.49) and (3.50) the electric field in the θ direction and magnetic field in the r direction can be derived.

$$E_\theta(r,\theta,z) = \begin{cases} -B_1 \frac{i\omega\mu}{k_{c1}^2} J_1(k_{c1}r) e^{i(\omega t - k_z z)} & 0 \leq r \leq a \\ B_1 \frac{i\omega\mu}{k_{c2}^2} \frac{J_0(k_{c1}a)}{K_0(k_{c2}a)} K_1(k_{c2}r) e^{i(\omega t - k_z z)} & r > a \end{cases} \tag{3.67}$$

$$H_r(r,\theta,z) = \begin{cases} B_1 \frac{ik_z}{k_{c1}^2} J_1(k_{c1}r) e^{i(\omega t - k_z z)} & 0 \leq r \leq a \\ -B_1 \frac{ik_z}{k_{c2}^2} \frac{J_0(k_{c1}a)}{K_0(k_{c2}a)} K_1(k_{c2}r) e^{i(\omega t - k_z z)} & r > a \end{cases} \tag{3.68}$$

From these equations, together with the condition from equations (3.64) and (3.65), the TE-modes can be calculated. The electric field inside a step-index fiber is simulated with Comsol in Chapter 4.3 and calculated analytically in Chapter 5.1.2.

4

Experimental Setup

In this chapter and Chapter 5, a variety of fibers were investigated. For convenience, the specifics of all the fibers can be found in Table 4.1. They are also shown in Figure 4.1 for the simple fiber, Figure 4.2 for the step-index fiber, Figure 4.3 for the photonic crystal bandgap fiber and Figure 4.4 for the three layer step-index fiber.

The incoming wavelength for all fibers is chosen to be $\lambda = 1.55 \cdot 10^{-6}$ m, because this is the propagation wavelength for the photonic crystal fiber, Fiber C. For simplicity this is chosen the same for all other fibers. For the simple fiber, Fiber A, the radius of the fiber is chosen in the range of a few wavelengths, to ensure multi-mode guidance. The refractive index is that of silica glass and conductor boundary conditions are applied. The structure of the step-index fiber, Fiber B, is based on an example from the book 'An Introduction to Optical Fibers'.[2] For the photonic crystal fiber, Fiber C, the specifics belong to the fiber HC-1550-02 (Thorlabs).[12] The values for Fiber E are based on Fiber D.

This chapter focuses on COMSOL Multiphysics [6] and the simulations of the fibers from Table 4.1.

Table 4.1: The radii, refractive indexes and boundary condition for the outer most layer of the different fibers that are used. PML is short for perfectly matched layer, which resembles an infinite domain outside of the fiber. With the simple fiber: Fiber A (Figure 4.1), the step-index fiber: Fiber B (Figure 4.2), the hollow core photonic crystal fiber HC-1550-02 and adjusted version: Fiber C and D, respectively (Figure 4.3) and three layer step-index fiber: Fiber E (Figure 4.4).

|	Fiber A	Fiber B	Fiber C	Fiber D	Fiber E
Radii	$R = 5 \cdot 10^{-6}$ m	$a = 43.5 \cdot 10^{-6}$ m $R = 62.5 \cdot 10^{-6}$ m	$R_1 = 4.75 \cdot 10^{-6}$ m $R_2 = 34.2 \cdot 10^{-6}$ m $R_3 = 35.4 \cdot 10^{-6}$ m $R_4 = 1.75 \cdot 10^{-6}$ m $R_5 = 3.8 \cdot 10^{-6}$ m	$R_1 = 3R_5 2 = 3.48 \cdot 10^{-6}$ m $R_2 = 9.5R_5 = 22.04 \cdot 10^{-6}$ m $R_3 = 10R_5 = 23.2 \cdot 10^{-6}$ m $R_4 = 1.044 \cdot 10^{-6}$ m $R_5 = 2.32 \cdot 10^{-6}$ m	$R_1 = 3.48 \cdot 10^{-6}$ m $R_2 = 22.04 \cdot 10^{-6}$ m $R_3 = 23.2 \cdot 10^{-6}$ m
Refractive indexes	$n = 1.45$	$n_1 = 1.458$ $n_2 = 1.427$	$n_{air} = 1$ $n_{glass} = 1.45$	$n_{air} = 1$ $n_{glass} = 1.45$	$n_1 = 1$ $n_3 = 1.45$ n_{eff} is adjustable
Boundary condition	Perfect electric conductor	Perfect electric conductor	PML	PML	PML
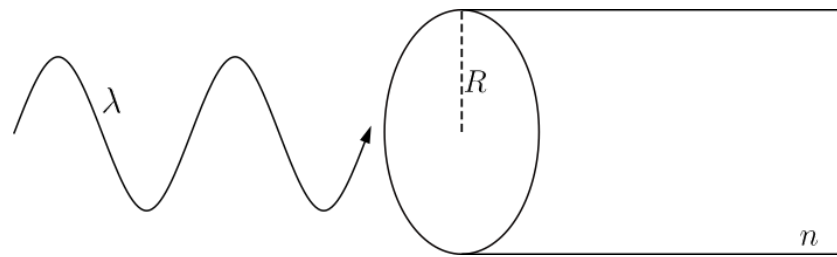
Figure 4.1: Schematic sketch of the simple fiber, Fiber A from Table 4.1, where $R = 10 \cdot 10^{-6}$ m, $n = 1.45$, $\lambda = 1.55 \cdot 10^{-6}$ m and with conductor boundary conditions.
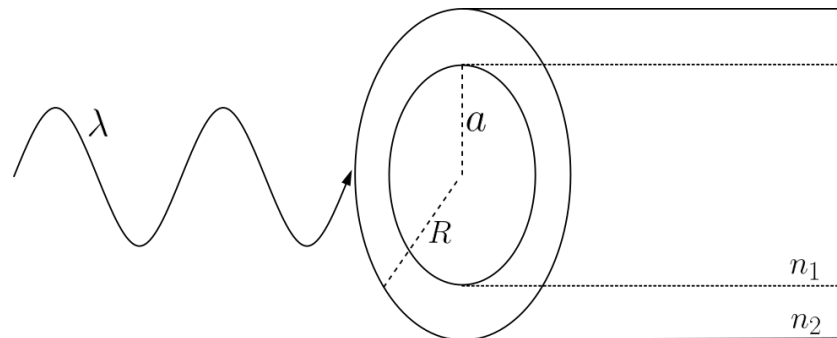

Figure 4.2: Schematic sketch of the step-index fiber, Fiber B from Table 4.1, where $R = 125 \cdot 10^{-6}$ m, $a = 62.5 \cdot 10^{-6}$ m, $n_1 = 1.451$, $n_2 = 1.45$ and $\lambda = 1.55 \cdot 10^{-6}$ m.
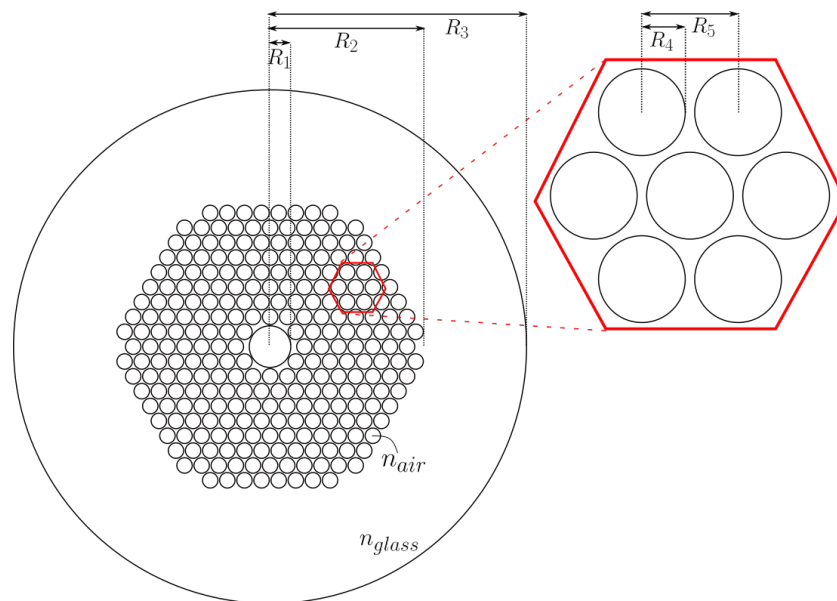

Figure 4.3: Schematic sketch of the cross-section of the Photonic Crystal Bandgap fiber, Fiber C from Table 4.1, where $R_1 = 4.75 \cdot 10^{-6}$ m, $R_2 = 34.2 \cdot 10^{-6}$ m, $R_3 = 35.4 \cdot 10^{-6}$ m, $R_4 = 1.75 \cdot 10^{-6}$ m, $R_5 = 3.8 \cdot 10^{-6}$ m, $n_{glass} = 1.45$ and $n_{air} = 1$ is the refractive index in all the holes, including the hole in the center.
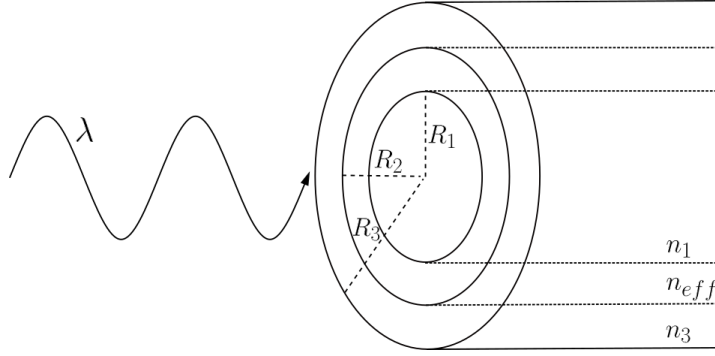
Figure 4.4: Schematic sketch of the three layer step-index fiber, Fiber D from Table 4.1, with $R_1 = 3.48 \cdot 10^{-6}$ m, $R_2 = 22.04 \cdot 10^{-6}$ m, $R_3 = 23.2 \cdot 10^{-6}$ m, $n_1 = 1$ and $n_3 = 1.45$. n_{eff} is a refractive index that can be adjusted to best match the photonic crystal fiber.

4.1. Comsol

The main tool that is used in the research for this report is COMSOL Multiphysics[6], which will be referred to as Comsol from now on.

4.1.1. Finite element method

Comsol simulations are based on the finite element method, also called FEM. FEM is a numerical method that is used to approximate the solution of systems of partial differential equations.[23] This is very useful, as many problems in physics can be written as a set of partial differential equations. In this case the partial differential equations that need to be solved are the Maxwell equations (3.1)-(3.4). To apply the FEM, the domain needs to be partitioned into smaller domains, called elements. The elements are defined by node points $\mathbf{x}_i$ with $i \in \{0, n\}$, with a total of $n + 1$ nodes.[20] In one dimension elements of the partition are then defined as intervals $[x_{j-1}, x_j]$ with $j \in \{1, n\}$. In two dimensions, the elements are usually triangles or sometimes quadrilaterals. The node points are then the corners of the triangles or quadrilaterals. FEM approximates the solution of the partial differential equations, in this case the electric field, with a linear combination of functions ψ_i.

$$E \approx \sum_{i=0}^{n} a_i \psi_i \tag{4.1}$$

with a_i the coefficients and ψ_i are called the basis functions. The ψ_i are assigned a value of 1 at node i and 0 for all the other nodes in the mesh.[26] Then the function between the nodes is usually linear, but can also be chosen as a different continuous function, such as polynomials of higher degrees. The total function ψ_i is continuous differentiable on the elements and continuous on the whole domain.[20] Methods with discontinuous functions also exist, but they will not be considered in this report. For a one dimensional domain in the x-direction with piecewise linear ψ_i, see Figure 4.5, the ψ_i are defined as follows

$$\psi_i(x) = \begin{cases} (x - x_{i-1}) / (x_i - x_{i-1}) & \text{if } x_{i-1} \leq x \leq x_i \\ (x_{i+1} - x) / (x_{i+1} - x_i) & \text{if } x_i \leq x \leq x_{i+1} \\ 0 & \text{otherwise} \end{cases} \tag{4.2}$$

where the elements are the intervals $[x_{j-1}, x_j]$ with $j \in \{1, n\}$, as mentioned earlier.
A function $f(x)$ can be approximated by linear interpolation on the subintervals ($[x_i, x_{i+1}]$), when the value of f is known at the nodes. The approximation is the continuous piecewise linear interpolant $\pi f(x)$.

$$\pi f(x) = \sum_{i=0}^{n} f(x_i) \psi_i(x) \tag{4.3}$$

There are also other ways to approximate $f(x)$, for example the L_2-projection.[20] The L_2 projection
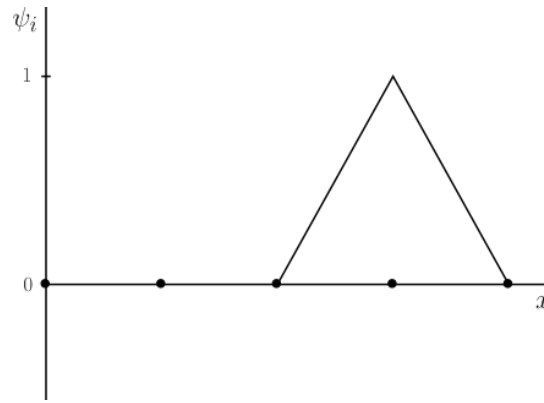
Figure 4.5: Example of a linear ψ_4 function for a 1D problem in the x-direction, with value 1 for the fourth node.

method projects the function f onto the function space with linear functions $(ax + b)$ for every interval $[x_i, x_{i+1}]$. This approximation does not have to be equal to the value of f at the nodes, unlike the interpolant.

In general a differential equation can be written as $L(\mathbf{u}) = f(\mathbf{x})$. In this case the Maxwell equations should be solved. In Comsol, the Maxwell equations are combined into one equation for the electric field. The following time independent differential equation needs to be solved to compute the modes.

$$\nabla \times (\nabla \times \mathbf{E}') - k_0 \varepsilon_r \mathbf{E}' = 0 \tag{4.4}$$

In Comsol this is called the electric wave equation. Where the time dependent solution is $\mathbf{E}(x, y, z, t) = \mathbf{E}'(x, y, z)e^{i\omega t}$. Comsol uses the ansatz that $\mathbf{E}'(x, y, z) = \tilde{\mathbf{E}}(x, y)e^{-i\beta z - \delta_z z}$, where β is the propagation constant and δz the attenuation constant. Equation (4.4) can be derived from the Maxwell equations. When taking the curl of equation (3.2), interchanging the time derivative and the curl and then inserting equation (3.4) gives

$$\nabla \times (\nabla \times \mathbf{E}) = -\mu \left(\nabla \times \frac{\partial \mathbf{h}}{\partial t} \right) = -\mu \frac{\partial}{\partial t} (\nabla \times \mathbf{E}) = -\mu \varepsilon \frac{\partial^2 \mathbf{E}}{\partial t^2} \tag{4.5}$$

This gives equation (4.4), with the time dependent solution give above, $\varepsilon = \varepsilon_0 \varepsilon_r$ and $k_0 = \frac{\omega}{c}$, where $c = \frac{1}{\sqrt{\mu_0 \varepsilon_0}}$ and assuming that $\mu = \mu_0$.[25]. Now the FEM is used to approximate $\mathbf{E}'$ from equation (4.4). First a variational formulation of equation (4.4) should be derived. In general a variational formulation is obtained by multiply the given differential equation with some test function $\mathbf{v}$ and then integrating. In this case this gives

$$\iiint_\Omega \nabla \times (\nabla \times \mathbf{E}') \cdot \mathbf{v} d\mathbf{x} = \iiint_\Omega k_0 \varepsilon_r \mathbf{E}' \cdot \mathbf{v} d\mathbf{x} \tag{4.6}$$

where Ω indicates the whole domain. This can be simplified to[20]

$$\iiint_\Omega (\nabla \times \mathbf{E}') \cdot (\nabla \times \mathbf{v}) \, d\mathbf{x} - \oiint_{\partial\Omega} (\nabla \times \mathbf{E}') \times \hat{\mathbf{n}} \cdot (\mathbf{v}) \, d\mathbf{x} = \iiint_\Omega k_0 \varepsilon_r \mathbf{E}' \cdot \mathbf{v} d\mathbf{x} \tag{4.7}$$

The function $\mathbf{E}'$ can then be approximated as $\mathbf{E}'_h$, where

$$\mathbf{E}'_h = \sum_{i=0}^{n} a_i \psi_i \tag{4.8}$$

the ψ_i are the basis functions that are explained earlier. They should be 1 at node i and 0 at all other nodes. a_i are the coefficients that need to be determined. The following has to hold for all possible test functions $\mathbf{v}$

$$\iiint_\Omega (\nabla \times \mathbf{E}'_h) \cdot (\nabla \times \mathbf{v}) \, d\mathbf{x} - \oiint_{\partial\Omega} (\nabla \times \mathbf{E}'_h) \times \hat{\mathbf{n}} \cdot (\mathbf{v}) \, d\mathbf{x} = \iiint_\Omega k_0 \varepsilon_r \mathbf{E}'_h \cdot \mathbf{v} d\mathbf{x} \tag{4.9}$$

v can be an infinite number of functions, as long as the integral from equation (4.6) exists and **v** should adhere to the boundaries of the problem. From this the coefficients a_i of $\mathbf{E}_h$ can be calculated, when the boundary conditions are known.[20] When the Galerkin method is used, the test functions **v** and $\mathbf{E}'_h$ can only be functions that are linear between the nodes and continuous over the whole domain. This function space can be spanned by a finite number of functions. Then this gives a system of equations which can be solved.

4.1.2. Settings

Comsol has a variety of modules, but here only the Wave Optics module is used. This module specialises in the analysis of electromagnetic waves with wavelengths in the micro- and nanometer range.[25] Within the Wave Optics module, the "Electromagnetic Waves, Frequency Domain" (*ewfd*) physics interface is used for all the simulations in this report.

Global definitions

In Comsol a few steps need to be taken to set up a Comsol model. In the beginning there is an option to add global definitions. This can be used to define parameter values. In future steps the parameter can be used instead of writing the specific value. This also makes it easier to change the values for one parameter all at the same time. An example of the parameter section can be found in Figure 4.6.

Name	Expression	Value	Description
r1	43.5[um]	4.35E-5 m	radius core
r2	62.5[um]	6.25E-5 m	radius cladding
lambda0	1.55[um]	1.55E-6 m	wavelength
f0	c_const/lambda0	1.9341E14 1/s	frequency
nco	1.458	1.458	refractive index
n2	1.427	1.427	refractive index cladding

Figure 4.6: Example of the parameter section in Comsol.

Geometry

The next step is to create the geometry. This is done in the component section. Material properties, such as the refractive indexes can be added to the different regions of the geometry. For the fibers that are simulated in this report, a 2D geometry of the cross section of the fibers can be used. Comsol has the option to extend the cross-section in the third dimension (over the z-axis) to create a 3D object. This can only be done, because the modes that exist in the fibers do not depend on the length of the fiber, so the solution does not change in the axial direction.

Boundary conditions

There is an option to add a perfectly matched layer (PML) as an artificial domain in the definitions tab. Perfectly matched layers can be used to resemble the boundary conditions for an infinite domain outside of the fiber. When the light enters a perfectly matched layer, it is absorbed and cannot reflect back into the fiber.[31] For this it is important that the mesh is dense enough inside the layer. This should be at least 5 mesh layers.[24] The typical wavelength of the PML should be selected and for all the fibers, the PML should be based on a cylindrical geometry. A PML is used for the photonic crystal fibers and the three layer step-index fiber, Fiber C, D and E. The exact setting of the used PMLs can be found in Chapter 4.4 and 4.5.

When the geometry is made, the boundary condition can be added. These are a part of the chosen physics interface, in this case *ewfd*. One boundary conditions that will be used is the Perfect Electric Conductor. This condition adheres to the following equation

$$\mathbf{n} \times \mathbf{E} = \mathbf{0} \tag{4.10}$$

where **n** is the normal vector of the boundary. This means that the electric field is completely in the direction normal to the boundary. As the electric field and magnetic field are always perpendicular for electromagnetic waves,[32] the magnetic field normal to the boundary has to be zero, $\mathbf{n} \cdot \mathbf{H} = 0$. This

condition is applied to Fiber A and B from Table 4.1, that are studied in Chapter 4.2 and 4.3. In *ewfd* there is the option to apply the Electric Wave Equation to parts of the domain and there is an option to set an initial value for the electric field. This value will then be used as the start guess for the solver. Also in the *ewfd* settings, the option should be selected to solve for a three-component vector.

Mesh
The mesh of the geometry is then created; this can be done automatically with a physics controlled mesh. This will be used for all the simulations in this report. When *ewfd* is selected as the the contributor, there is an option to base the maximum size of a mesh element on the study. The mesh will then have a maximum element size that is $\frac{1}{5}$ of the smallest wavelength that the study uses.[25] The mesh is used to indicate for which points the study should be calculated. An example of a mesh can be seen in Figure 4.10.

Study and results
The last step is to select the study and fill in the study details. The study indicates what Comsol should calculate. The study that is used in these experiments is the mode analysis. This study looks for the modes of the fiber. A parametric sweep can be used to conduct the study over specific values for a certain parameter.
When the study is conducted, it is important to distinguish the propagating modes, as Comsol can also show modes that do not propagate. There are many different ways to display the result. For example in a table, with a 2D surface graph, or in 1D at $y = 0$. The results that Comsol gives, are calculated using the finite element method.

4.2. Simple fiber Comsol

In this section Fiber A from Table 4.1 is simulated in Comsol. The values for the radius, wavelength, frequency and refractive index are defined in the parameter section of Comsol, see Table 4.2.

Table 4.2: Parameters section in Comsol for the simulation of Fiber A from Table 4.1.

Name	Expression	Value	Description
r	5[um]	$5 \cdot 10^{-6}$ m	radius
lambda0	1.55[um]	$1.55 \cdot 10^{-6}$ m	wavelength
f0	c_const/lambda0	$1.9341 \cdot 10^{14}$ 1/s	frequency
n	1.45	1.45	refractive index

Then the geometry is made, see Figure 4.7. The material is given the earlier defined refractive index $n = 1.45$.
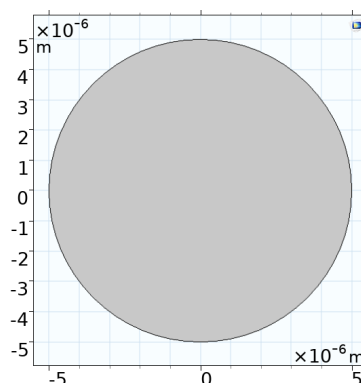

Figure 4.7: The geometry of the Comsol simulation of Fiber A from Table 4.1.

In *ewfd* the boundary conditions are added. The wave equation for the electric field (equation (4.4)) and an initial value of $\mathbf{E} = \mathbf{0}$ as start guess are applied to the whole domain. The boundary is assigned perfect electric conductor properties (equation (4.10)).

The mesh is set to have "extremely fine" elements. The *ewfd* is used as contributor and the maximum element size is based on the study, as explained in Chapter 4.1.2. The mesh is shown in Figure 4.8.
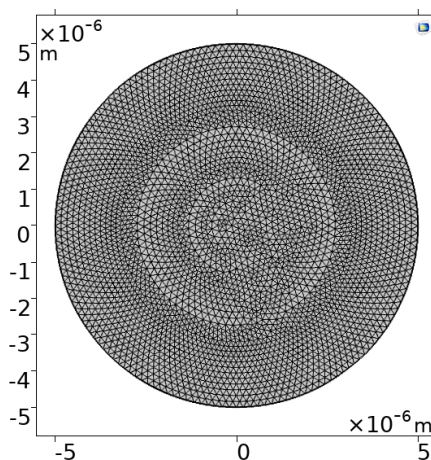

Figure 4.8: The mesh used for the Comsol simulation of Fiber A from Table 4.1, with 6550 domain elements and 160 boundary elements.

The mode analysis study is computed for a total of 16 modes. The frequency $f_0 = \frac{c_0}{\lambda}$ that is used, was defined earlier as a parameter (Table 4.2) and the modes are sought for around the refractive index $n = 1.45$.

4.3. Step-index fiber Comsol

Next, a step-index fiber is simulated in Comsol. This is Fiber B, for which the specifications are given in Table 4.1. The parameters, as they are defined in Comsol, can be seen in Table 4.3.

Table 4.3: Parameters section in Comsol for the simulation of Fiber B from Table 4.1.

Name	Expression	Value	Description
r1	43.5[um]	$4.35 \cdot 10^{-5}$ m	radius core
r2	62.5[um]	$6.25 \cdot 10^{-5}$ m	radius cladding
lambda0	1.55[um]	$1.55 \cdot 10^{-6}$ m	wavelength
f0	c_const/lambda0	$1.9341 \cdot 10^{14}$ 1/s	frequency
nco	1.458	1.458	refractive index
n2	1.458	1.427	refractive index cladding

The geometry that is made in Comsol is shown in Figure 4.9. For the material of the inner circle, the refractive index is set at $n_1 = 1.458$ and for the cladding or ring, the refractive index is $n_2 = 1.427$.
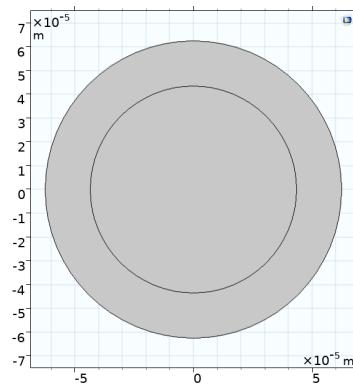

Figure 4.9: The geometry of the Comsol simulation of Fiber B from Table 4.1.

Then the settings for *ewfd* are selected. The electric wave equation (4.4) is applied to the whole domain and the initial value is set to 0. For all the outer boundaries the conditions for a Perfect Electric Conductor (equation (4.10)) are added.
The physics controlled mesh is selected with the mesh size set to "extremely fine" and *ewfd* is used as contributor. The maximum element size is depending on the study. Figure 4.10 shows the final mesh.
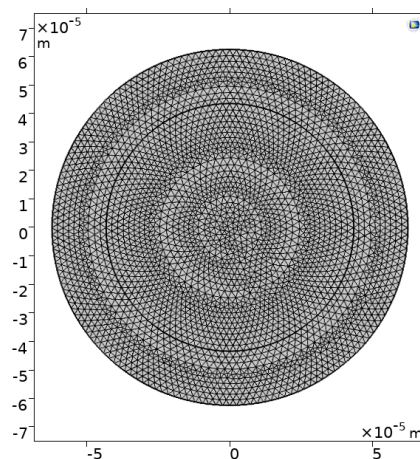

Figure 4.10: The mesh used for the Comsol simulation of Fiber B from Table 4.1, with 6156 domain elements and 272 boundary elements.

Finally, the settings for the study are inserted. The mode analysis study is used with mode analysis frequency f_0, that was defined as a parameter (Table 4.3). A total of 9 modes are computed around $n_1 = 1.450$.

## 4.4. Photonic crystal fiber

Finally, the goal is to investigate the photonic crystal bandgap fiber HC-1550-02, that was also used in the article from B. Wan et al.[31] The fiber that is being investigated is fiber C from Table 4.1. In the process of simulating this fiber a lot of issues have been encountered. The parameters that are defined in Comsol to model this fiber can be seen in Table 4.4.
The first geometry that was made with Comsol can be seen in Figure 4.11. A perfectly matched layer is used with a thickness of $6\lambda = 9.3 \cdot 10^{-6}$ m and typical wavelength $\lambda/n_{glass} \approx 1.07 \cdot 10^{-6}$ m. The geometry type of the perfectly matched layer is set to cylindrical.
The electric wave equation (4.4) is again applied to the whole domain and initial values are set to be 0. The outer boundary is set to be a Perfect Electric Conductor, equation (4.10).

Table 4.4: Parameters defined in Comsol for the simulation of Fiber C from Table 4.1.

Name	Expression	Value	Description
pitch	3.8[um]	$3.8 \cdot 10^{-6}$ m	pitch
vert_disp	tan(60[degree])*pitch/2	$3.2909 \cdot 10^{-6}$ m	vertical displacement
r_hole	3.5[um]/2	$1.75 \cdot 10^{-6}$ m	radius air holes
r_core	9.5[um]/2	$4.75 \cdot 10^{-6}$ m	radius core
r_clad	70.8[um]/2	$3.54 \cdot 10^{-5}$ m	radius cladding
n_holes	10	10	number holes in radius
wavelength	1.55[um]	$1.55 \cdot 10^{-6}$ m	wavelength
n_air	1	1	refractive index airholes
n_glass	1.45	1.45	refractive index glass
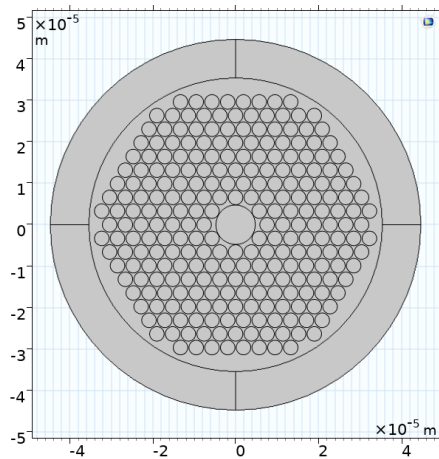
Figure 4.11: The geometry of the Comsol simulation of Fiber C from Table 4.1, with a perfectly matched layer with thickness $6\lambda = 9.3 \cdot 10^{-6}$ m.

The mesh is set to be physics-controlled and have normal sized elements. *ewfd* is selected as the contributor and element size is based on the study. The mesh is very dense. This can be seen in Figure 4.12. The perfectly matched layer has a mapped mesh. This means that elements with four edges are used (quadrilaterals). In this case they make up a cylinder, so they have two curved edges. The remaining mesh has triangular shaped mesh elements.
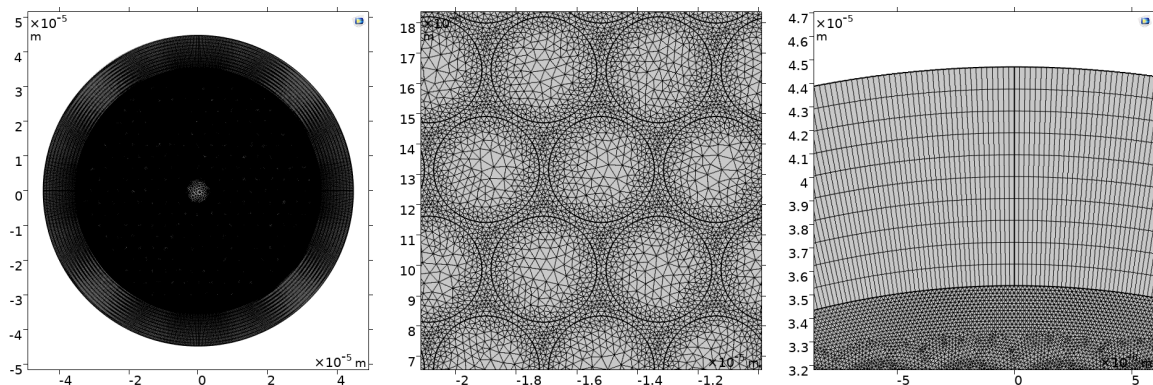
(a) The mesh on the whole domain.

(b) The mesh in the air hole region.

(c) The mesh in the perfectly matched layer.

Figure 4.12: The mesh used for the Comsol simulation of Fiber C from Table 4.1, with 255884 domain elements and 18131 boundary elements.

Then a mode analysis is computed for 6 modes and the mode analysis frequency was set to be c/λ. The modes are sought for around an effective refractive index of 0.995. This is the same setting that B. Wan et al.[31] used. This is not an actual refractive index, as they should always be larger than 1, but it is the complex refractive index. The complex refraction index is related to the attenuation of the fiber.[34] The results from the simulation can be found in Chapter 5.2.3. In short, these are not the results that are expected and they do not match the findings from B. Wan et al.[31]. The modes are not centered in the core of the fiber.

After contacting Comsol support, it turned out that the HC-1550-02 could not be modeled with Comsol. This geometry was a very sensitive design, meaning that it only works for very specific parameters. With the help of Comsol support, a new, similar hollow core photonic crystal fiber was modeled, with a few changes. This new model was supplied by Thomas Esselink, a master student at the TU Delft, who used this model for his research.[10] Fiber D from Table 4.1 has the dimensions of the new photonic crystal fiber. The circular core is replaced with a star shaped core. This new shape is based on an article from Kunimasa Saitoh and Masanori Koshiba.[30] The new model is much more stable than the old one, so it works for a larger range of parameter values. The parameter values that are used in this new model can be seen in Table 4.5.

Table 4.5: Parameters defined in Comsol for the simulation of Fiber D from Table 4.1.

Name	Expression	Value	Description
lda0	1.55[um]	$1.55 \cdot 10^{-6}$ m	wavelength
lambda	2.32[um]	$2.32 \cdot 10^{-6}$ m	pitch
dNormalized	0.9	0.9	ratio air holes pitch
d	dNormalized*lambda	$2.088 \cdot 10^{-6}$ m	air hole diameter
nAir	1	1	refractive index air holes
nGlass	1.45	1.45	refractive index air glass
nEffExp	0.987	0.987	effective refractive index
nRadialGlass	sqrt(nGlass^2-nEffExp^2)	1.062	
ldaPML	lda0/nRadialGlass	$1.4592 \cdot 10^{-6}$ m	wavelength PML
tPML	ldaPML	$1.4592 \cdot 10^{-6}$ m	thickness PML
f0	c_const/lda0	$1.9341 \cdot 10^{14}$ 1/s	frequency
N	8	8	air holes in radius

The adjusted geometry is modeled in Comsol, see Figure 4.13. The perfectly matched layer has a thickness and typical wavelength of $1.4592 \cdot 10^{-6}$ m and a cylindrical type geometry.
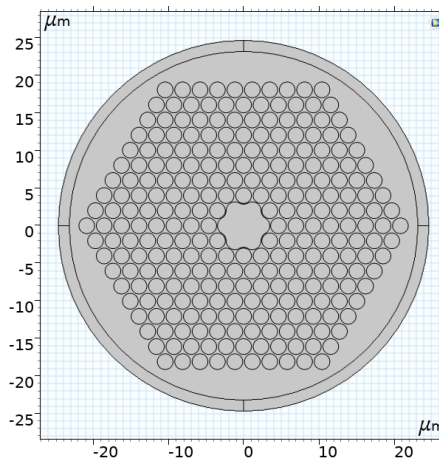

Figure 4.13: The geometry of the Comsol simulation of Fiber D from Table 4.1, with a perfectly matched layer with thickness $1.4592 \cdot 10^{-6}$ m.

Perfect electric conductor conditions are applied to the most outer layer and the electric wave equation is set on the whole domain (equations (4.10) and (4.4)). The initial values are set at 0 V/m.
The mesh is calculated with normal element size and again with *ewfd* as contributor. The maximum element size is based on the study, as explained in Chapter 4.1.2. Figure 4.14 shows the mesh for different parts of the geometry. Similar as for Fiber C, the perfectly matched layer has a mapped mesh. The rest of the mesh is made up of triangular elements.

(a) The mesh on the whole domain.

(b) The mesh in the air hole region.
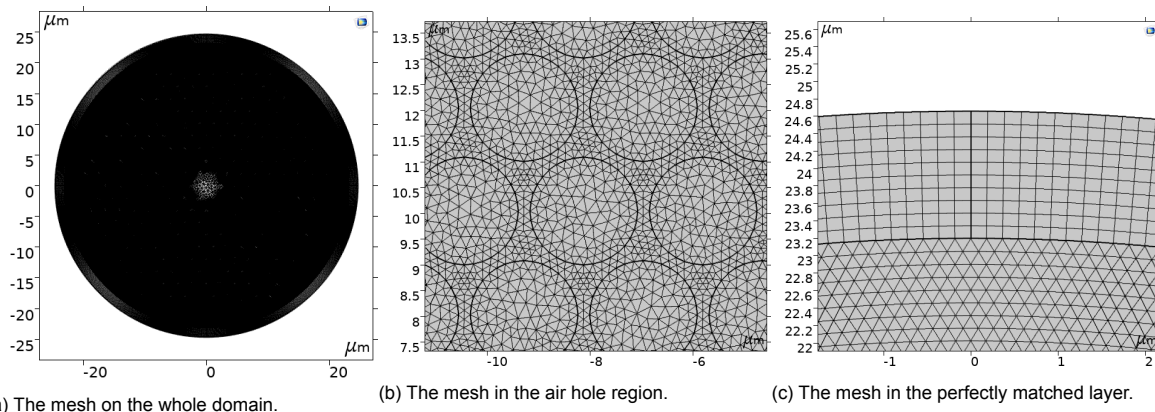
(c) The mesh in the perfectly matched layer.

Figure 4.14: The mesh used for the Comsol simulation of Fiber D from Table 4.1, with 135168 domain elements and 11293 boundary elements.

Next a mode analysis is computed to find 6 modes with mode analysis frequency $f_0 = c/\lambda$. The modes are sought for near an effective refractive index of 0.987. This was set by Comsol support. From experience, the effective refractive index should be just below one, to find guiding modes. The result from this study are shown and discussed in Chapter 5.2.3. For this fiber, the modes do propagate and are confined to the core.

4.5. Three layer step-index fiber

The last step is estimate the photonic crystal fiber with an easier fiber, Fiber E from Table 4.1, for which the field could be computed analytically. The three layer step-index fiber is chosen to try to approximate the photonic crystal fiber with star-shape core, Fiber D from Table 4.1. The three radii are chosen to be the core radius, radius of the air hole region and the cladding radius of Fiber D. The refractive index of the core is the same and the refractive index of the outer layer is that of the cladding of Fiber D. The refractive index of the middle layer should be determined to best match the modes of Fiber D. In general the goal is to get a mode confined to the core.

As an estimate the refractive index of the middle layer is chosen to have a real part that is the average of the two surrounding layers, so Real$(n_{eff}) = (n_1 + n_3)/2 = 1.225$. The refractive index is also given an imaginary part, because this simulates the attenuation. A parametric sweep is done for the imaginary part from 0 up to 1 with steps of 0.1.
Fiber E from Table 4.1 is then modeled in Comsol. The parameter section that is used can be found in Table 4.6.

Table 4.6: Parameters defined in Comsol for the simulation of Fiber E from Table 4.1.

Name	Expression	Value	Description
lambda0	1.55[um]	$1.55 \cdot 10^{-6}$ m	wavelength
f0	c_const/lda0	$1.9341 \cdot 10^{14}$ 1/s	frequency
r1	3.48[um]	$3.48 \cdot 10^{-6}$ m	radius core
r2	22.04[um]	$2.204 \cdot 10^{-5}$ m	radius middle layer
r3	23.2[um]	$2.32 \cdot 10^{-5}$ m	radius cladding
n1	1	1	refractive index core
n3	1.45	1.45	refractive index cladding
neff_real	1.225	1.225	real refractive index middle layer
nEffExp	0.987	0.987	effective refractive index
tPML	labda0/sqrt(n3^2-nEffExp^2)	$1.4592 \cdot 10^{-6}$ m	thickness PML
neff_im	0.5*i	$0.5i$	imaginary refractive index middle layer

The geometry is shown in Figure 4.15. A perfectly match layer is used with the same settings as used for the simulation of Fiber D, a cylindrical geometry type and a thickness and typical wavelength of $1.4592 \cdot 10^{-6}$ m.
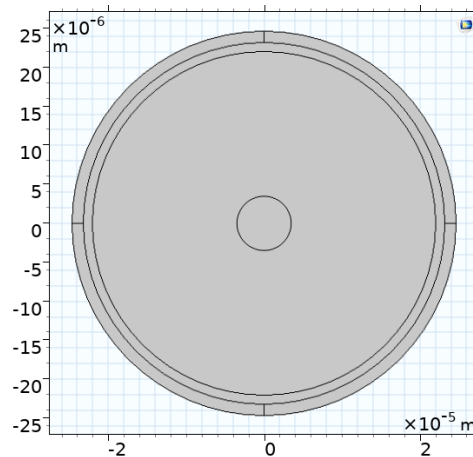

Figure 4.15: The geometry of the Comsol simulation of Fiber D from Table 4.1, with a perfectly matched layer with thickness $1.4592 \cdot 10^{-6}$ m.

The electric wave equation (4.4) is applied to the whole domain; electric conductor boundary conditions (equation (4.10) are applied to the outer boundary of the perfectly matched layer and the initial values for the electric field are set to 0. A physics-controlled mesh is used with normal element size and *ewfd* as contributor. The maximum element size is based on the study. The resulting mesh can be seen in Figure 4.16.

(a) The mesh on the whole domain.

(b) The mesh in and around the core.

(c) The mesh in the perfectly matched layer, outer layer and partly of the middle layer.
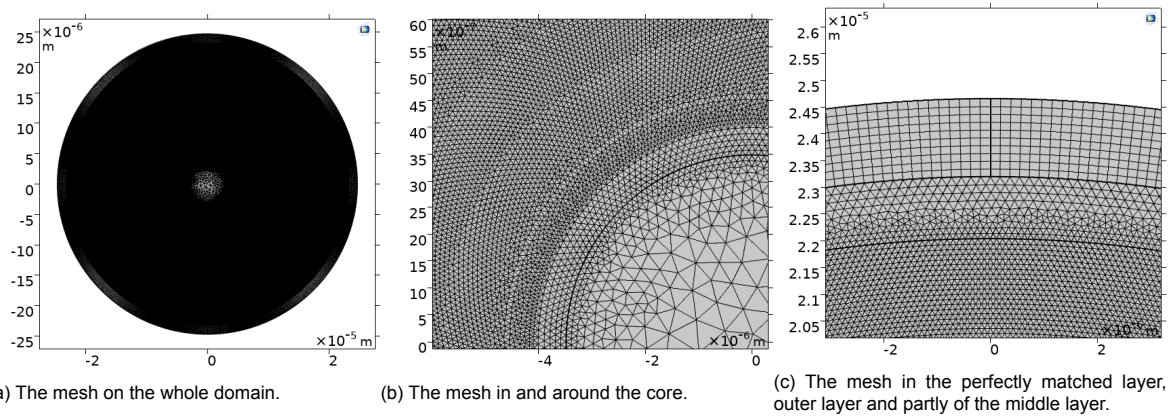
Figure 4.16: The mesh used for the Comsol simulation of Fiber E from Table 4.1, with 360638 domain elements and 3020 boundary elements.

Lastly the mode analysis study is computed. The mode analysis frequency is $f_0 = c/\lambda$, a total of 6 modes are computed around 0.987. This is firstly done with the earlier mentioned parametric sweep over the imaginary part of the refractive index from 0 to 1 with steps of 0.1. After this another sweep is done for values of $\text{Im}(n_{eff})$ from 10 to 100 with step size 10. The results can be found in Chapter 5.2.4.

5

Results and Discussion

5.1. Analytical

This chapter contains the results and a discussion of the analytical calculations of the electric field for a simple fiber and for a step-index fiber.

5.1.1. Simple Fiber

The electric field of the simple fiber, Fiber A from Table 4.1, is calculated analytically. Equations 3.35, 3.36 and 3.38 from Chapter 3.2.1 are used to get the analytical solution for the TE-modes and equations 3.41, 3.42 and 3.44 from Chapter 3.2.2 for the TM-modes. The following values are chosen conveniently at $H_1 = 1$ and $E_1 = 1$, as they do not influence the distribution of the field. The wavelength is calculated with $\omega = \frac{2\pi c}{\lambda n}$ and the following constant values are used $\mu = 4\pi \cdot 10^{-7}$ kgms^{-2}A^{-2} and $c = 3 \cdot 10^8$ ms^{-1}. The wavelength of the incoming wave is set at $\lambda = 1.55 \cdot 10^{-6}$ m, see Figure 4.1. This was the same in the Comsol simulations from Chapter 4.2. The result is plotted with Python. Figure A.1 shows 16 of the TE$_{mn}$ modes and Figure A.2 shows 16 of the TM$_{mn}$ modes The fields are calculated for the same points as the Comsol simulation of Fiber A, from Chapter 4.2.

Looking at Figure A.1, for the TE$_{mn}$ modes, it can be seen that the modes where n = 1, have one maximum in the radial direction, modes with n = 2 have two radial maxima, etc. In general it seems that there are n radial maxima. In the radial direction something similar can be noticed. The m = 0 modes have no azimuthal maxima or minima. The field is constant when varying over θ, but keeping r fixed. This also becomes clear when looking at equations (3.35) and (3.36). For m = 0, the electric field in the r direction is zero. The only non constant term that remains is $J'_m(k_c r)$ in the equation for the electric field in the θ direction. Therefore, the field for m = 0 only varies with r. For m = 1 there are two maxima, for m/2 there are four maxima and so on. It can be concluded that there are 2m maxima in the azimuthal direction.
Similar to the TE$_{mn}$ modes, the TM$_{mn}$ modes have n maxima in the radial direction and m/2 maxima in the azimuthal direction, see Figure A.2.

In all cases, the electric field is zero in the centre, except for the m = 1 modes. This is because the derivative of all Bessel functions is zero at $r = 0$, except for m = 1. First consider all modes with $m > 1$. The Bessel functions with index larger than one, are zero at $r = 0$, but also their derivative is zero, see Figure 3.3. Therefore, the electric field in the r and θ direction is zero, see equations (3.35), (3.36), (3.41) and (3.42). For the m = 0 modes, the derivative of the Bessel function is still zero, but the Bessel function itself is not. However, with m = 0 the electric field also vanishes. Only for m = 1, the derivative of the electric field is non zero. This leaves an electric field in the θ direction for the TE modes and in the r direction for the TM modes.
The results that are found match the electric fields shown by E. Jensen.[15]

5.1.2. Step Index Fiber

The electric field of the TE-modes of the step-index fiber, Fiber B from Table 4.1, is also calculated analytically and then plotted with Python. The specific values that are used can also be found in Figure 4.2. These are the same values that are used for the Comsol simulations of Fiber B in Chapter 4.3. Equations (3.64) and (3.65) are used to derive the values for $\kappa_1 = k_{c1}a$ and $\kappa_2 = k_{c2}a$, before it is possible to compute the electric field. As these equations are too complex, because of the multiple Bessel equations, the values need to be derived numerically. Figure 5.1 shows the functions that need to be solved ($f_1 = f_2$) to find κ_1. The following expressions are used for f_1 and f_2.

$$\begin{cases} f_1 = \dfrac{J_1(\kappa_1)}{\kappa_1 J_0(\kappa_1)} \\[4mm] f_2 = \dfrac{K_1\left(\sqrt{u^2-\kappa_1^2}\right)}{\sqrt{u^2-\kappa_1^2}K_0\left(\sqrt{u^2-\kappa_1^2}\right)} \end{cases} \quad \text{with} \quad u = \sqrt{k_0^2 a^2 \left(n_1^2 + n_2^2\right)} \tag{5.1}$$
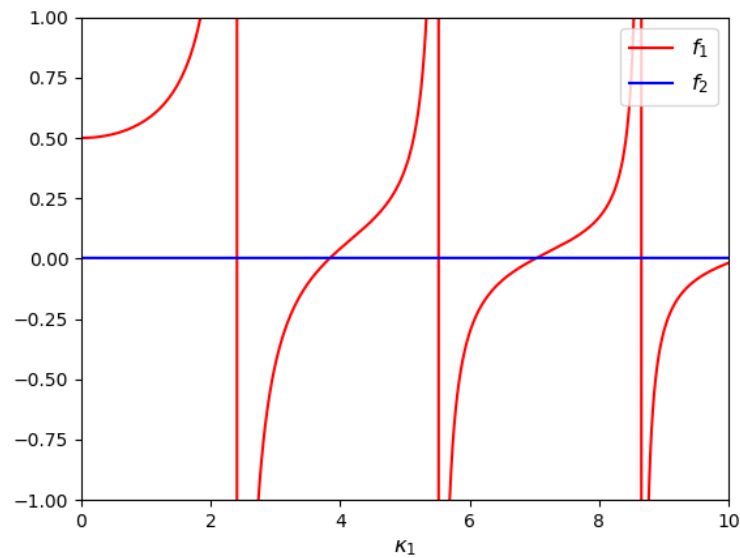

Figure 5.1: Functions f_1 and f_2 from equation (5.1), plotted against κ_1.

From this figure, it can be seen that the first intersection is around 2.5 and the second near 3.5. With the 'nsolve' command from sympy, the solution of nonlinear equations can be estimated numerically in Python. This is used to compute the value of κ_1. When 2.5 is given as a start estimate for κ_1, the value of $\kappa_1 \approx 3.82$ is found, so the intersection at 2.5 is not found. This raises the question if there is an actual intersection. The function seems to have a jump discontinuity here. Looking at the Bessel functions in Figure 3.3, it can be seen that $J_0 = 0$ around $x = 2.5$. This is the cause of the discontinuity. With the value $\kappa_1 \approx 3.82$, the results of the norm of the electric field are plotted and shown in Figure 5.2. For convenience and without loss of generality, the field is calculated with $B_1 = 1$.
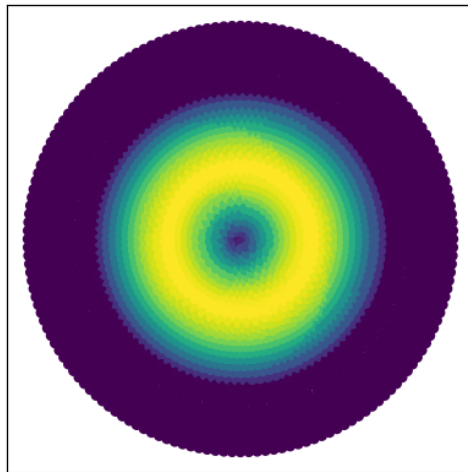
Figure 5.2: The analytical solution of the norm of the electric field (V/m) for the step-index fiber with $\kappa_1 = 3.82$, made with Python. For a fiber with the R, a, n_1, n_2 and λ that are specified in Figure 4.2.

This mode is confined to the core, which is to be expected as the result of total internal reflection. For small enough angles, the light is totally reflected at the interface, according to Snell's law.[18]

5.2. Comsol

5.2.1. Simple Fiber

The modes of Fiber A from table 4.1 are computed according to the steps from Chapter 4.2. It took 15 seconds to compute the study. The data of the electric field for all 16 modes is exported from Comsol. Python is used to plot the modes from this data, see the Appendix, Figure A.3. This shows the norm of the electric field. The absolute value of the electric field in the direction of propagation is illustrated in Figure A.4 and absolute value of the magnetic field in propagation direction in Figure A.5.

From these figures, it is expected that modes 1, 2, 3, 4, 7, 8, 12, 13, 15 and 16 are TE modes, as they do not have an electric field in the z-direction. Mode 11 has a very small, but not negligible electric field. Modes 5, 6, 9, 10 and 14 have no magnetic field in the propagation direction. Therefore, these modes are probably TM modes. Oddly enough, mode 11 has a significant electric and magnetic field in the propagation direction. However, if the norm of the electric field of mode 11 is compared to mode 10, these are similar, but rotated over an angle. From this, it can be expected that mode 11 is a TM mode like mode 10.
It can be noticed that all modes are shown twice, but rotated over an angle, except for mode 9 and 10. This might be, because mode 9 and 10 have cylindrical symmetry. For the other modes, the two matching modes correspond to two different polarisations. With a superposition of these two polarisations, all other polarisations of that mode can be made.[15]

These simulated modes from Figure A.3 can be compared to the earlier results of the analytically determined modes from Chapter 5.1.1, Figure A.1 and A.2. It can be seen that modes 1 and 2 have the distribution of the TE_{12} mode. Mode 3 and 4 do not match any of plotted TE or TM modes. They have a similar form as the TE_{21} and TE_{31}, but with a total of eight azimuthal maxima instead of four and six respectively. From this, it can be assumed that mode 3 and 4 are TE_{41} mode. So modes 1,2,3 and 4 are indeed TE modes as expected from the electric field in the z-direction. Mode 5 and 6 match the TM_{21} mode, 7 and 8 with the TE_{31} mode. This is also in line with the earlier remark that mode 5 and 6 are TM modes and mode 7 and 8 are TE modes. Mode 9 is the TE_{01} mode, mode 10 and 11 are TM_{11} modes. This confirms the assumption that 11 is a TM mode like 10, but still raises the question why the magnetic field in the propagation direction is so large. Mode 12 and 13 have the same field as TE_{21} mode, mode 14 is a TM_{01} mode and mode 15 and 16 are TE_{11} modes.
It can now also be noticed that the modes that are not shown twice, mode 9 and 14, are all the modes with m = 0. These fields have only a transverse electric field in the r direction or θ direction for TM and

TE modes, respectively.

5.2.2. Step-index Fiber

The results of the study of Fiber B from table 4.1 are displayed and discussed here. The results are obtained following the steps from Chapter 4.3. It took 16 seconds to compute this study. The data is again exported from Comsol and Python is used to plot the fields. Figure A.6 shows the norm of the electric field. Figures A.7 and A.8 show the absolute value of the electric field and magnetic field in the z-direction, E_z and H_z respectively.

The fields of all fibers are contained inside the core, as is expected from total internal reflection. The modes all seem to have an electric and magnetic field in the propagation direction, which means that these are hybrid modes.

Figure 5.3 shows a comparison between the analytical solution from Chapter 5.1.2 and the seventh Comsol mode. Both are evaluated over the x-axis, so $y = 0$. For the Comsol result, this is done with a 2D cut line. This means that the solution is given for points on a chosen line, in this case the line $y = 0$. The analytical solution is just calculated for $y = 0$. Both the results are normalised by dividing by the maximum value, which means that the maximum will be one. The plot is made in Python.
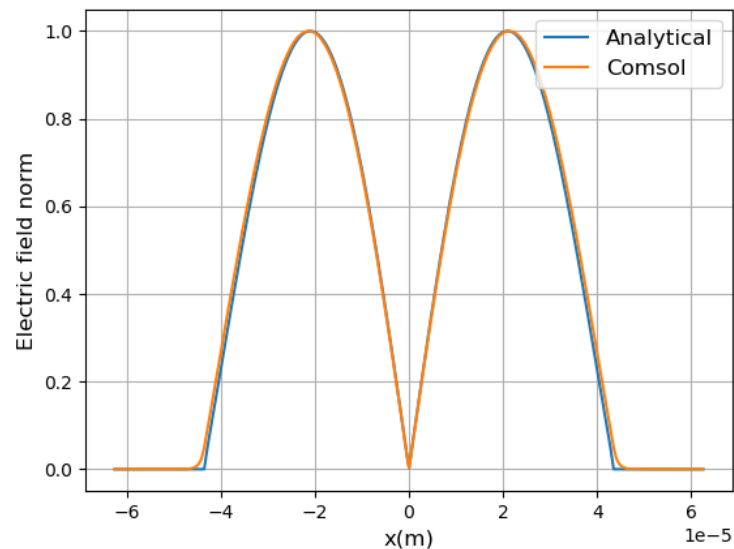

Figure 5.3: The analytical solution of the norm of the electric field for the step-index fiber, Fiber B from Table 4.1 at $y = 0$ and norm of the electric field of the seventh Comsol mode from Figure A.6 also at $y = 0$, both plotted against the x-coordinate.

From this figure, it can be seen that the Comsol result and analytical solution match. Figure 5.4 shows the error of Comsol compared to the analytical solution. This is the absolute value of the difference of the normalised functions. There is not a big difference between the two results. There are small differences around $x = -4 \cdot 10^{-5}$ m and $x = 4 \cdot 10^{-5}$ m. This is at the interface of the two media, $r = a$. This could be a result of the way that FEM calculates the field near the boundaries. However, the Comsol simulations all seemed to be hybrid modes and this one matches with the analytical TE mode.
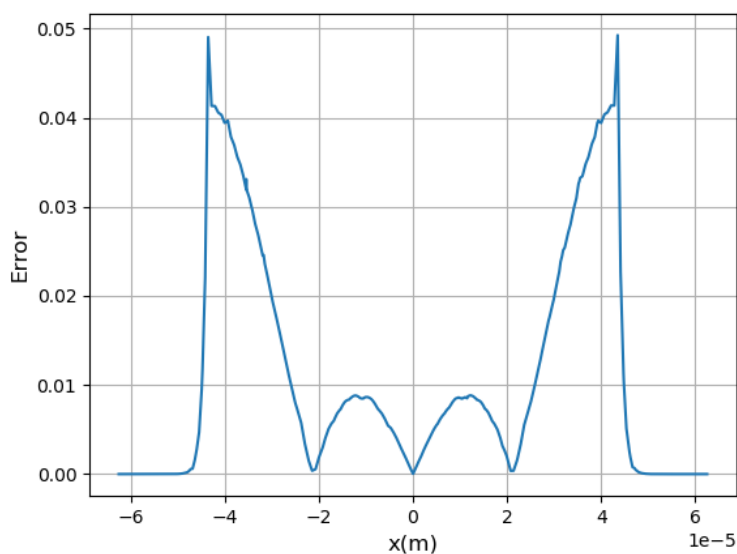
Figure 5.4: The absolute value of the difference between the normalised analytical solution and the normalised Comsol solution of the step-index fiber, Fiber B from Table 4.1.

5.2.3. Photonic crystal fiber

The modes of Fiber C from Table 4.1 are computed by taking the steps from Chapter 4.4. It took 20 minutes and 41 seconds to compute the study. This is much longer than the simulations of the simple fiber and step-index fiber. The mesh of the photonic crystal fiber contains more elements than the meshes used for the simple and step-index fiber. This causes the large difference in computation time. The norm of the electric field is plotted for all modes with Python,[14] see Figure 5.5. Table 5.1 shows the attenuation for the different modes.

Table 5.1: The attenuation constant per m in dB for the six modes from Figure 5.5.

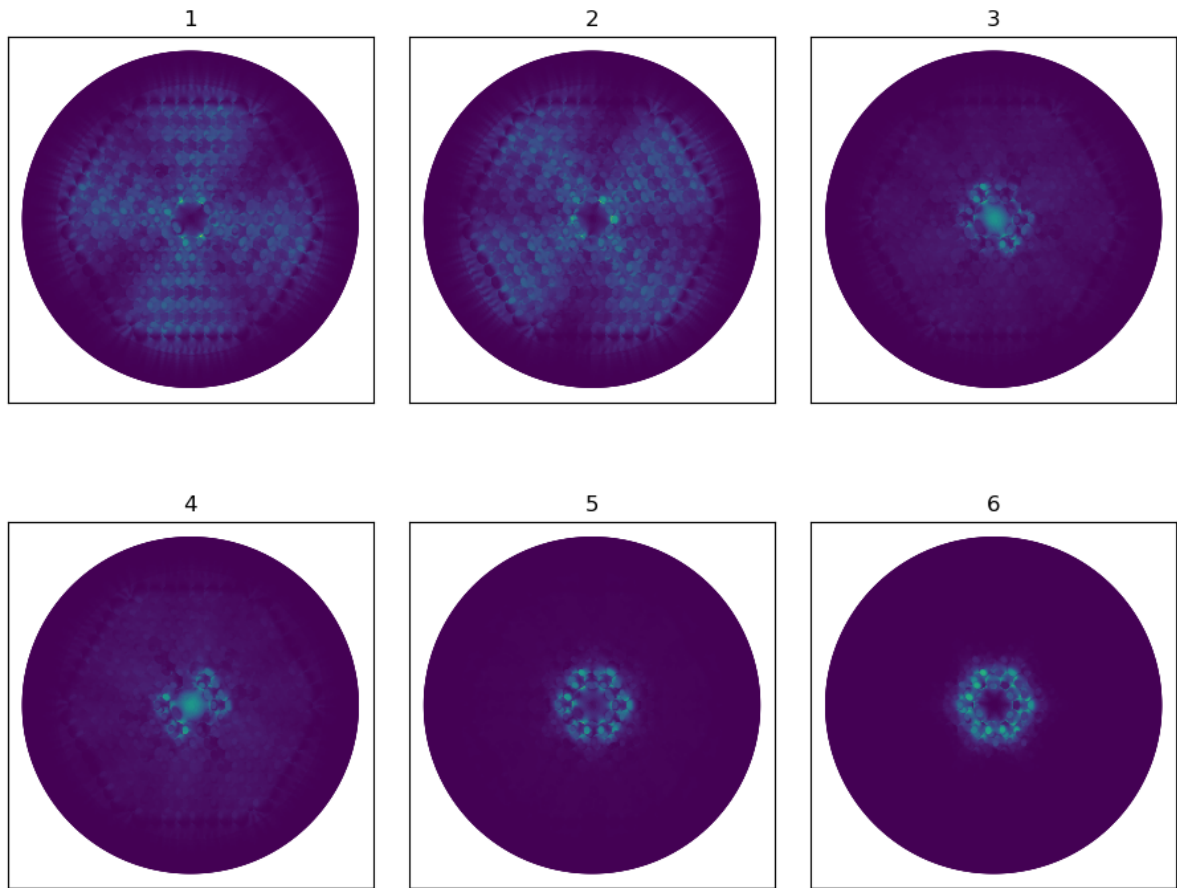| Mode	1	2	3	4	5	6
Attenuation (rad/m)	$5.253 \cdot 10^4$	$5.253 \cdot 10^4$	$1.375 \cdot 10^4$	$1.375 \cdot 10^4$	$5.786 \cdot 10^2$	$1.142 \cdot 10^1$

Figure 5.5: The norm of the electric field of the first six mode of fiber C from Table 4.1 that are computed with Comsol.

These modes are not concentrated in the core of the fiber as desired and shown by Wan et al.[31] Instead, a large part of the electric field exists in the cladding, which is not desirable for gas sensing. From Table 5.1, it can also be seen that the attenuation is very large. Therefore, the calculated modes will not propagate. After multiple tries to find propagating modes, Comsol support was contacted. They indicated that the simulations with this geometry are not reliable and this geometry should not be used.

The second photonic crystal fiber that is simulated is Fiber D from Table 4.1. The modes are computed in Comsol with the steps from Chapter 4.4. The computation took 14 minutes and 23 seconds. Python is used to display the norm of the electric field, see Figure 5.6. The attenuation for these simulated modes is shown in Table 5.2.

Table 5.2: The attenuation constant per m in dB for the six modes from Figure 5.6.

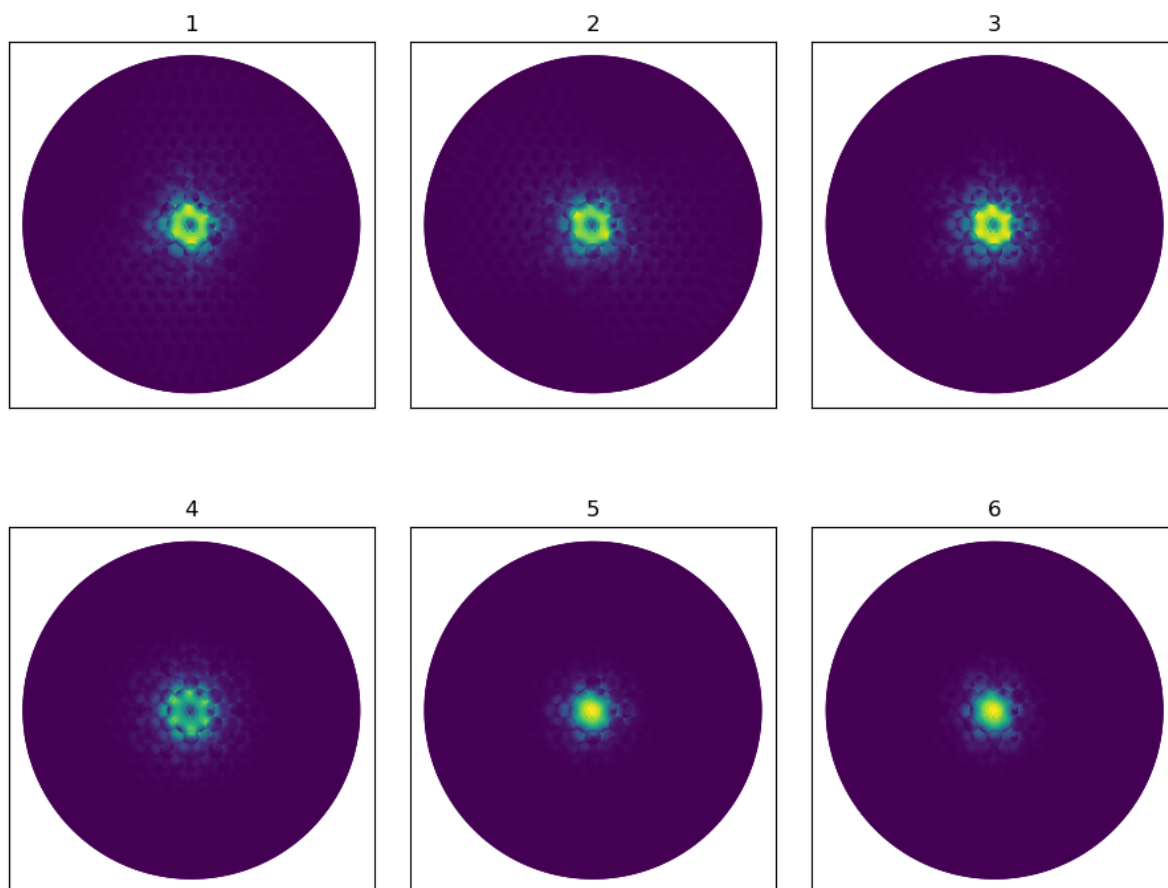| Mode	1	2	3	4	5	6
Attenuation (rad/m)	$1.579 \cdot 10^3$	$1.579 \cdot 10^3$	$8.027 \cdot 10^1$	$2.857 \cdot 10^1$	$5.443 \cdot 10^{-1}$	$5.444 \cdot 10^{-1}$

Figure 5.6: The norm of the electric field of the first six modes computed with Comsol for Fiber D from Table 4.1.

In this case, there are modes that are largely confined to the core, mode 5 and 6. The attenuation for these modes is also smaller than 1, so these modes do propagate. In general all modes for this fiber, Fiber D are much more confined to the core than the modes from Fiber C from Table 4.1, that are visible in Figure 5.5. The modes shown in Figure 5.6 are the desired modes, that are expected from a photonic crystal fiber.[31] When a gas sample is added inside the hollow core, the light can interact better with the sample. As the electric field is almost completely confined inside the core, the intensity of the light will be higher. The low attenuation means that the light can travel over a long distance inside the fiber, which realises a longer interaction length with the gas sample.

5.2.4. Three layer step-index fiber
The attenuation of the three layer step-index fiber, Fiber E from 4.1 is computed according to the steps from Chapter 4.5. It took 13 min and 46 second to calculate the six modes for $Im(n_{eff}) = 0.9$. This is not much faster than the computation of the modes for the photonic crystal fiber.
The attenuation was calculated for all six modes for all eleven values of the imaginary refractive indexes from the parametric sweep from 0 to 1 with steps of 0.1. Table 5.3 shows the minimum attenuation for all the different refractive indexes over the six modes.

Table 5.3: The minimum attenuation constant per m in dB for the different imaginary parts of the refractive indexes n_{eff} for Fiber E from Table 4.1.

$Im(n_{eff})$	0	0.1	0.2	0.3	0.4	0.5	0.6	0.7	0.8	0.9	1
Attenuation ($\cdot 10^4$ rad/m)	12.87	11.54	10.27	9.327	8.701	8.294	8.033	7.869	7.773	7.727	6.961

It can be seen that the attenuation is very high and the modes will not propagate. The attenuation decreases slightly for higher values of the imaginary part of the refractive index. The norm of the electric field for the modes with the lowest attenuation of refractive indexes $\text{Im}(n_{eff}) = 0.9$ and $\text{Im}(n_{eff}) = 1$ are shown in Figure 5.7.
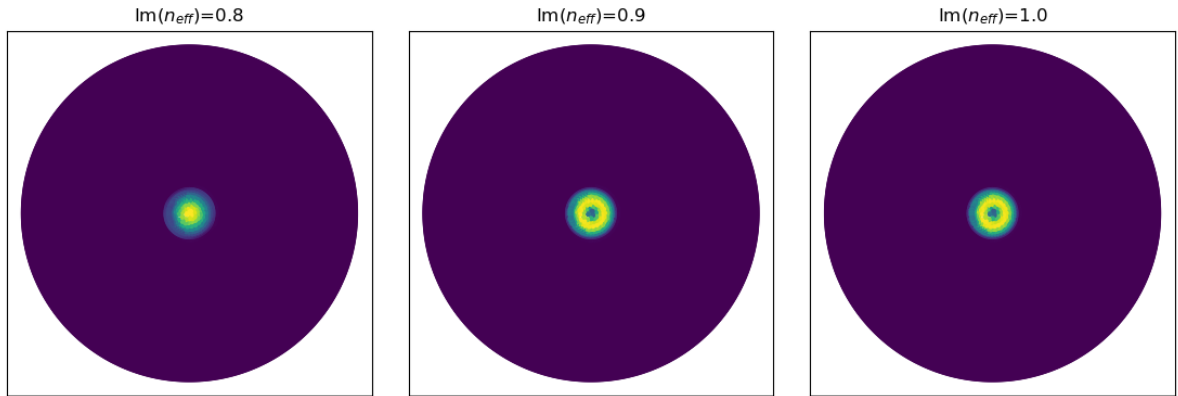

Figure 5.7: The norm of the electric field for the three layer step-index fiber, Fiber E from Table 4.1, with $\text{Im}(n_{eff}) = 0.8$, 0.9 and 1.0 for the mode with the lowest attenuation.

The field of the mode with $\text{Im}(n_{eff}) = 0.8$ looks more like the field from the photonic crystal fiber than the other two modes. All the modes are confined in the core, but the modes from $\text{Im}(n_{eff}) = 0.9$ and $\text{Im}(n_{eff}) = 1.0$ do not have the maximum in the center of the core. For gas sensing this is not desired, as the field should be mainly focused in the center to have a high interaction rate.

A second parametric sweep is computed to see if the attenuation decreases even more for higher values of $\text{Im}(n_{eff})$. The minimum attenuation for each $\text{Im}(n_{eff})$ of the six calculated modes is displayed in Table 5.4.

Table 5.4: The minimum attenuation constant per m in dB for the different imaginary parts of the refractive indexes n_{eff} for Fiber E from Table 4.1.

$\text{Im}(n_{eff})$	10	20	30	40	50	60	70	80	90	100
Attenuation ($\cdot 10^1$ rad/m)	2478	293.0	86.45	36.45	18.66	10.85	6.830	4.556	3.214	2.343

The attenuation is again decreasing for increasing $\text{Im}(n_{eff})$. The decrease becomes slower as $\text{Im}(n_{eff})$ gets higher. Figure 5.8 shows the mode of $\text{Im}(n_{eff}) = 100$ with the lowest attenuation 23.43 rad/m.
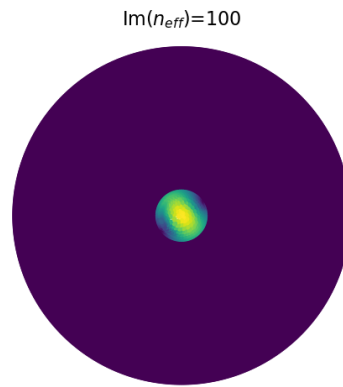
Figure 5.8: The norm of the electric field for the three layer step-index fiber, Fiber E from Table 4.1, with $\text{Im}(n_{eff}) = 100$ for the mode with the lowest attenuation.

This mode is not exactly the same as the mode in the photonic crystal fiber (Figure 5.6), but it does have a maximum intensity in the center of the fiber.

$$6$$

Conclusion

6.1. Simple fiber

The analytical equations for the electric field inside a simple fiber, that are derived in Chapter 3.2, match with the fields found by E. Jensen.[15] The modes of the simple fiber, that are simulated with Comsol, have similar distributions of the electric field norm as the analytical result showed. However, Comsol seems to show all TE$_{mn}$ and TM$_{mn}$ with $m \neq 0$ twice. This could be because of the polarisation direction. With two different polarisation direction, all other possible polarisations can be made by a superposition of the two. The electric field in the propagation direction is zero for all the TE modes, as expected. However, there is one TM mode for which the magnetic field in the propagation direction is not negligible. It is recommended to look further into what exactly Comsol does to compute the modes

6.2. Step-index fiber

The analytical equation for the step-index fiber matches with the simulations for the step-index fiber that were computed with Comsol. The Comsol solutions were all hybrid modes. However, at least one of the modes matches with the analytically calculated TE mode. This again confirms that the field in the direction of propagation that Comsol gives, might not be correct or should be interpreted differently. The Comsol solution has a slight derivation from the analytical solution at the interface between the two layers of the step-index fiber. This could be the result of the meshing at the interface. In that case mesh refinement techniques can be used to get better results. One option is to reduce the element size.

6.3. Photonic crystal fiber

It was not possible to simulate the HC-1550-02 photonic crystal fiber with Comsol, as was done by B. Wan et al.[31]. The modes that are simulated for this fiber are not confined in the core and have a very large attenuation, which indicates that they will not propagate. The lowest attenuation that was found for this fiber was $1.142 \cdot 10^1$dB rad/m. It is advised to simulate a different photonic crystal fiber as Comsol also was not able to produce a working model. Therefore, a similar fiber is used that is based on an article from K. Saitoh and M. Koshiba.[30] For this fiber a mode with an attenuation constant in dB per meter was found of $5.443 \cdot 10^{-1}$ rad/m. This mode was largely confined to the core. From this it can be concluded that this fiber indeed has modes that propagate and are confined inside the core. This is useful for gas sensing, as a high interaction rate and long interaction length between the gas and the light can be realised.

6.4. Three layer step-index fiber

The goal was to find a three layer step-index fiber with a similar mode as the photonic crystal fiber. The norm of the electric field is calculated with Comsol for a variation of refractive indexes for the middle layer. Especially, the imaginary part of the refractive index is varied. The results showed that the attenuation is very large for all modes with imaginary parts between 0 and 100. However, the

attenuation decreased with increasing imaginary part of the refractive index. The attenuation constant in db per m was still too high for the mode to propagate, namely 23.43 rad/m. The attenuation constant might be low enough for even higher imaginary parts of the refractive index. However, it is questionable if it is possible to ever realise a medium with such refraction index.

For further research, it is advised to estimate the refractive index of the middle layer on the structure of the air holes in the cladding of the photonic crystal fiber, for example by determining the effective refraction index of the photonic region. Besides this, it is wise to gather more information about complex refractive indexes. In this research, only the imaginary part of the refraction index of the middle layer is varied. It could also be beneficial to look into the influence of the real part of the refraction index or the radius of the middle layer.

In general, it could be beneficial to be able to estimate the modes of photonic crystal fibers with the modes of three layer step-index fibers. The computation time in Comsol is not much faster for the three layer step-index fiber that was used, but it would be possible to analytically calculate the electric field. In this report the analytical solution for the simple fiber and step-index fiber are derived. This could also be done for the three layer step-index fiber, which means that an analytical estimation of the electric field inside photonic crystal fibers could be made.
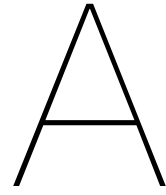
A
Appendix
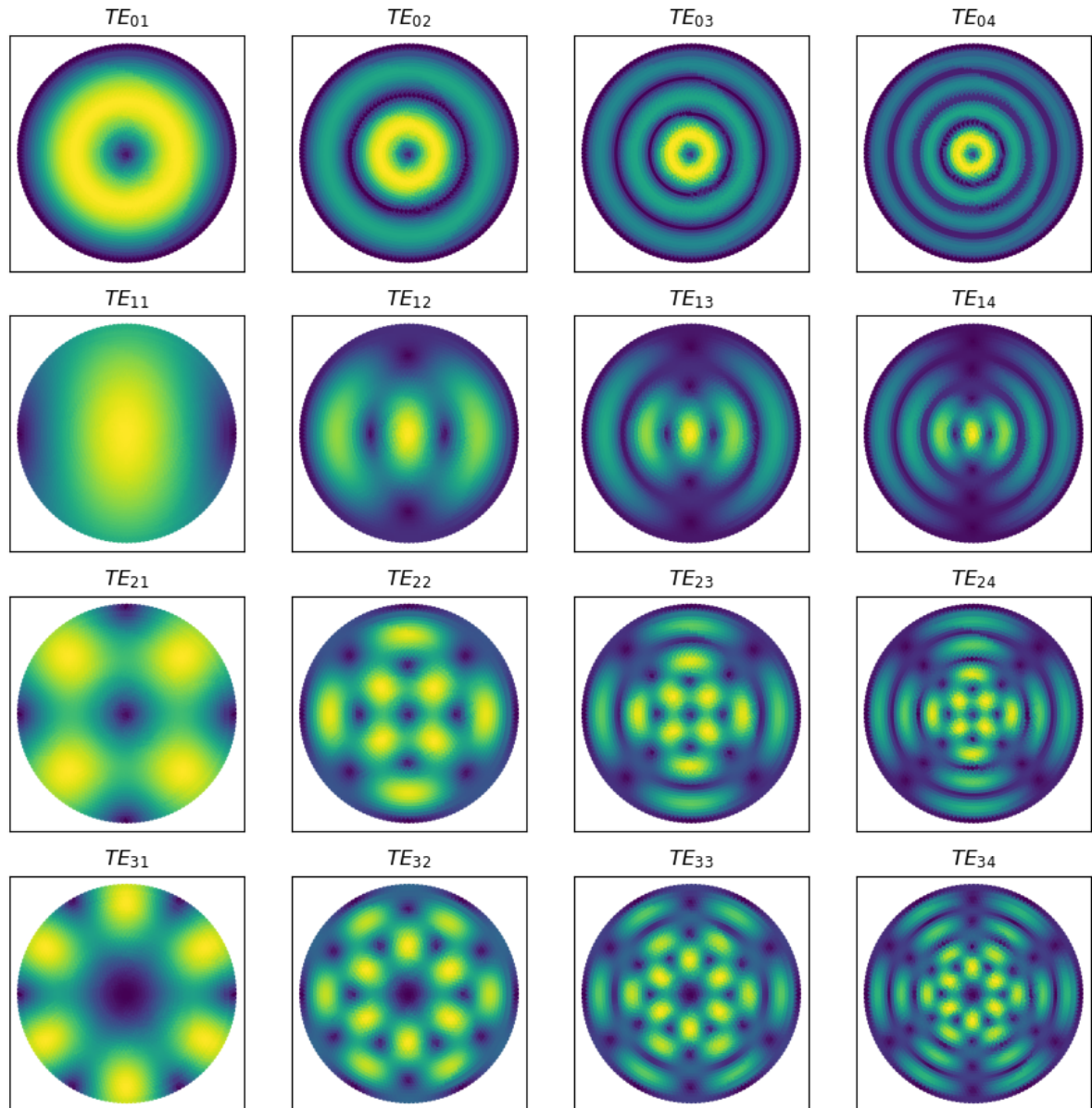
A.1. Simple fiber analytical

Figure A.1: Analytical solution for the TE_{mn} modes of the simple fiber, Fiber A from Table 4.1, plotted with python.
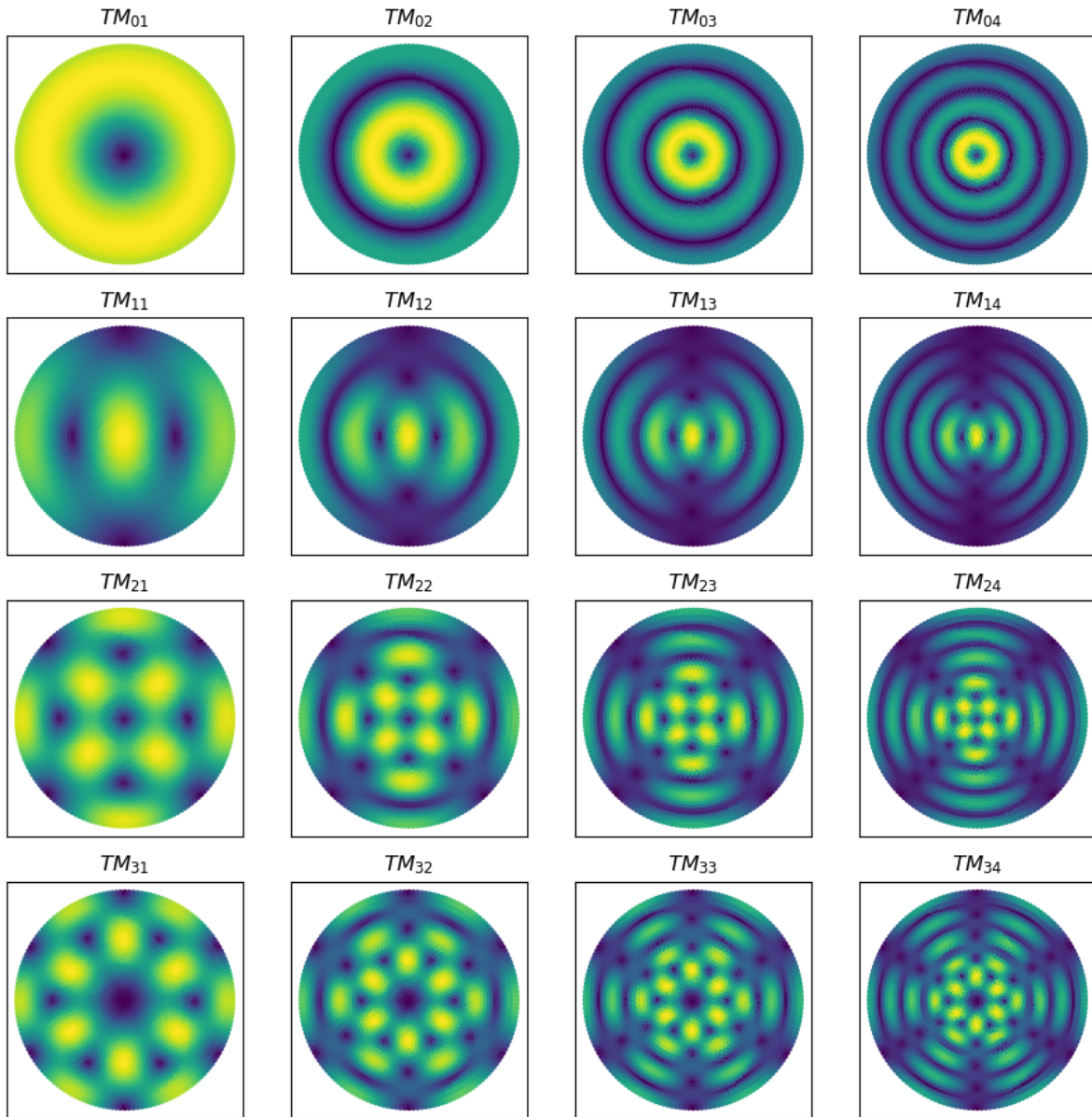
Figure A.2: Analytical solution for the TM_{mn} modes of the simple fiber, Fiber A from Table 4.1, plotted with python.
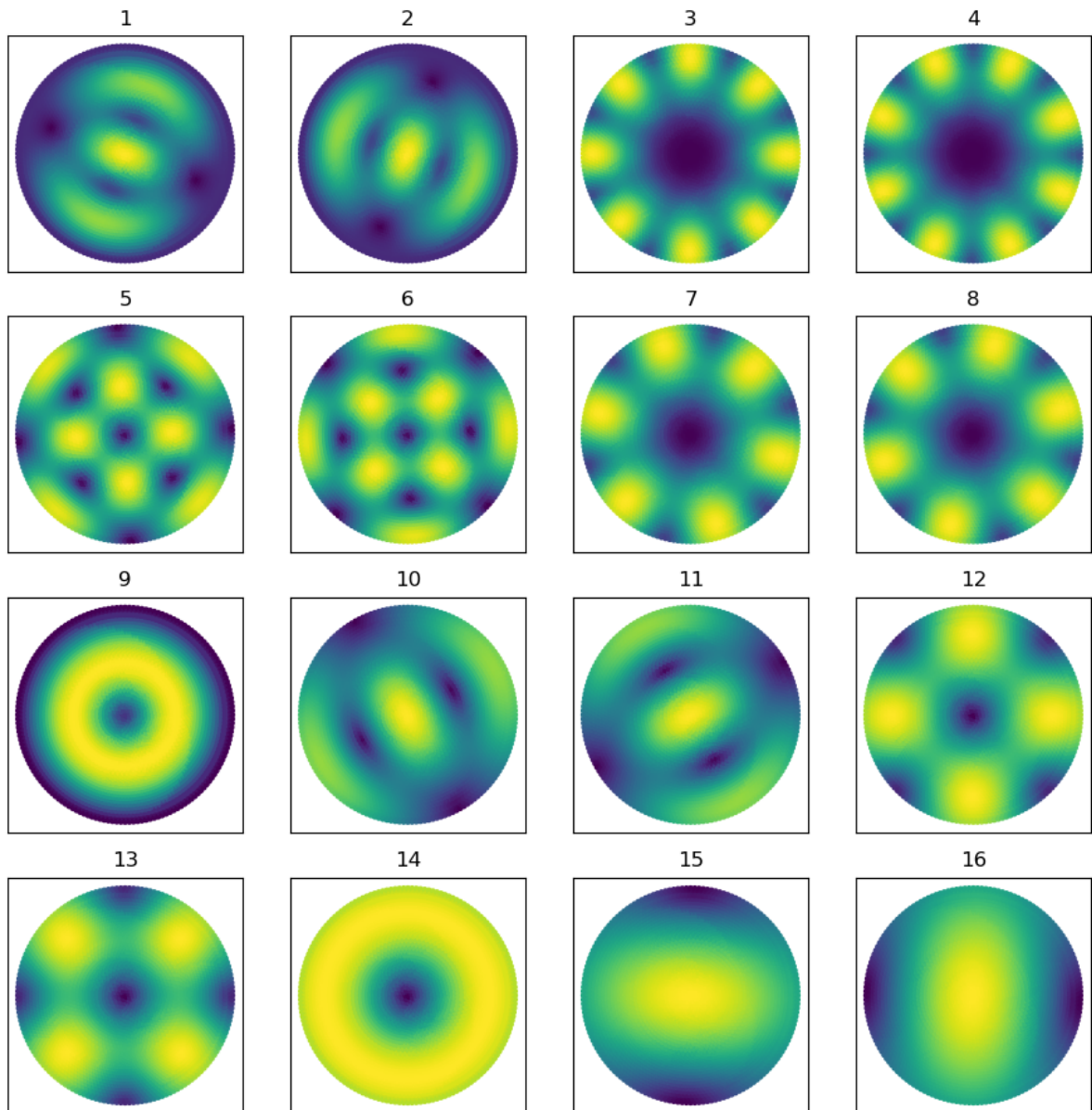
A.2. Simple fiber Comsol

Figure A.3: Results from the Comsol simulation for the norm of the electric field in V/m for the first 16 modes of Fiber A from Table 4.1, plotted with Python[14].
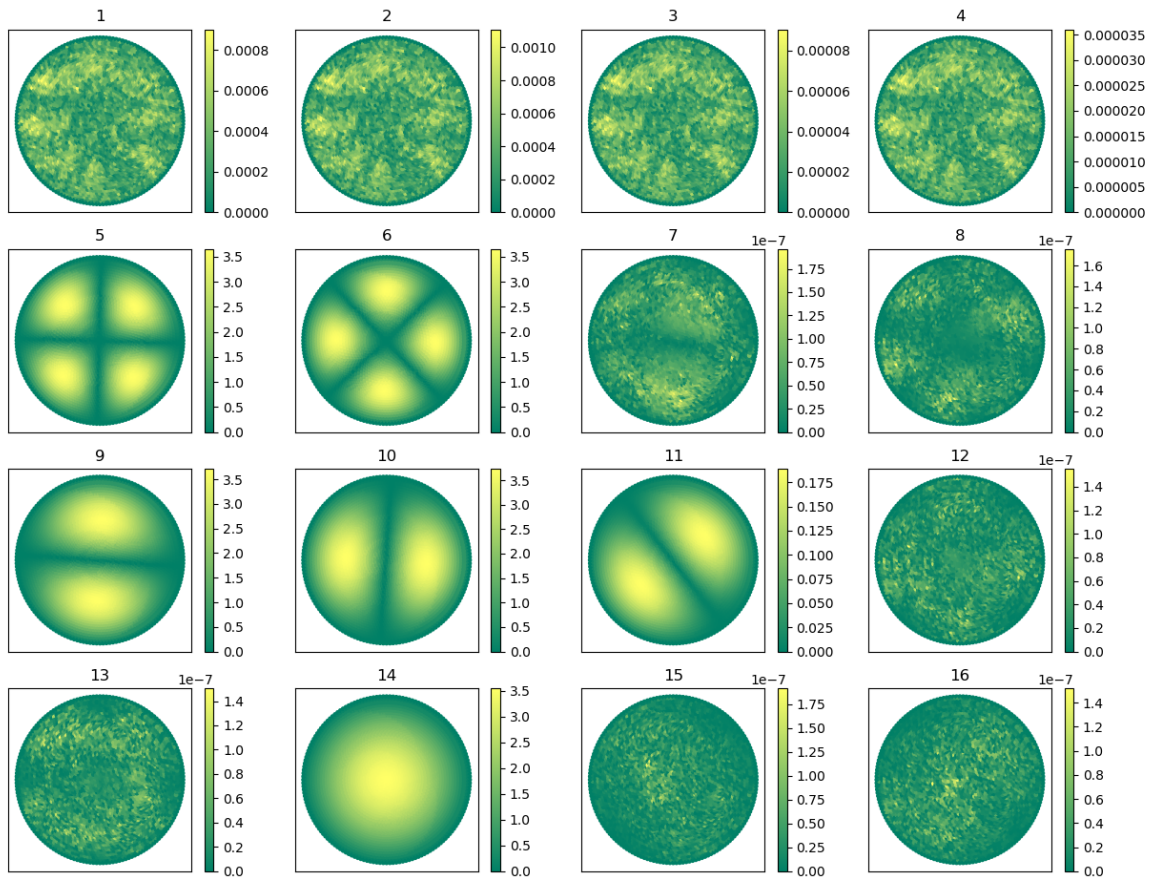
Figure A.4: Results from the Comsol simulation of the absolute value of the electric field in the direction of propagation E_z in V/m for the first 16 modes Fiber A from Table 4.1, plotted with Python[14].
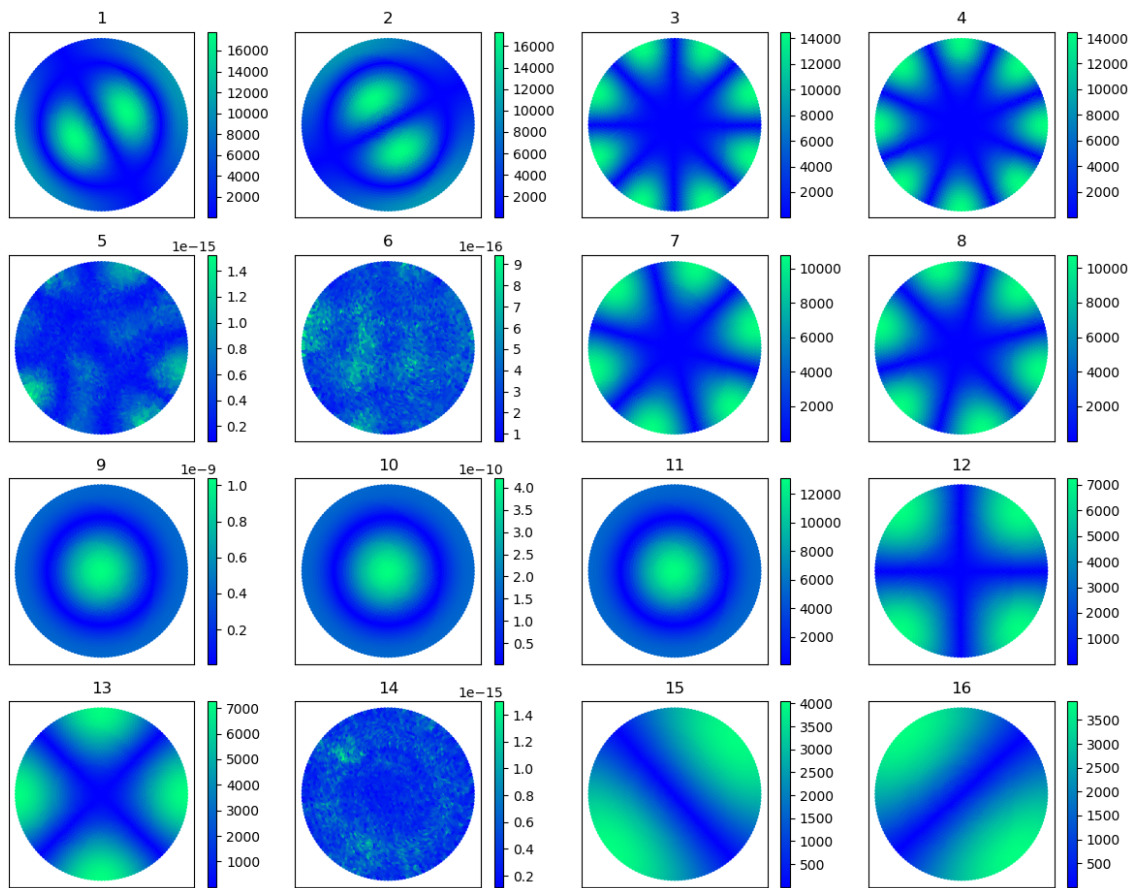
Figure A.5: Results from the Comsol simulation of the absolute value of the magnetic field in the direction of propagation H_z in A/m for the first 16 modes Fiber A from Table 4.1, plotted with Python[14].
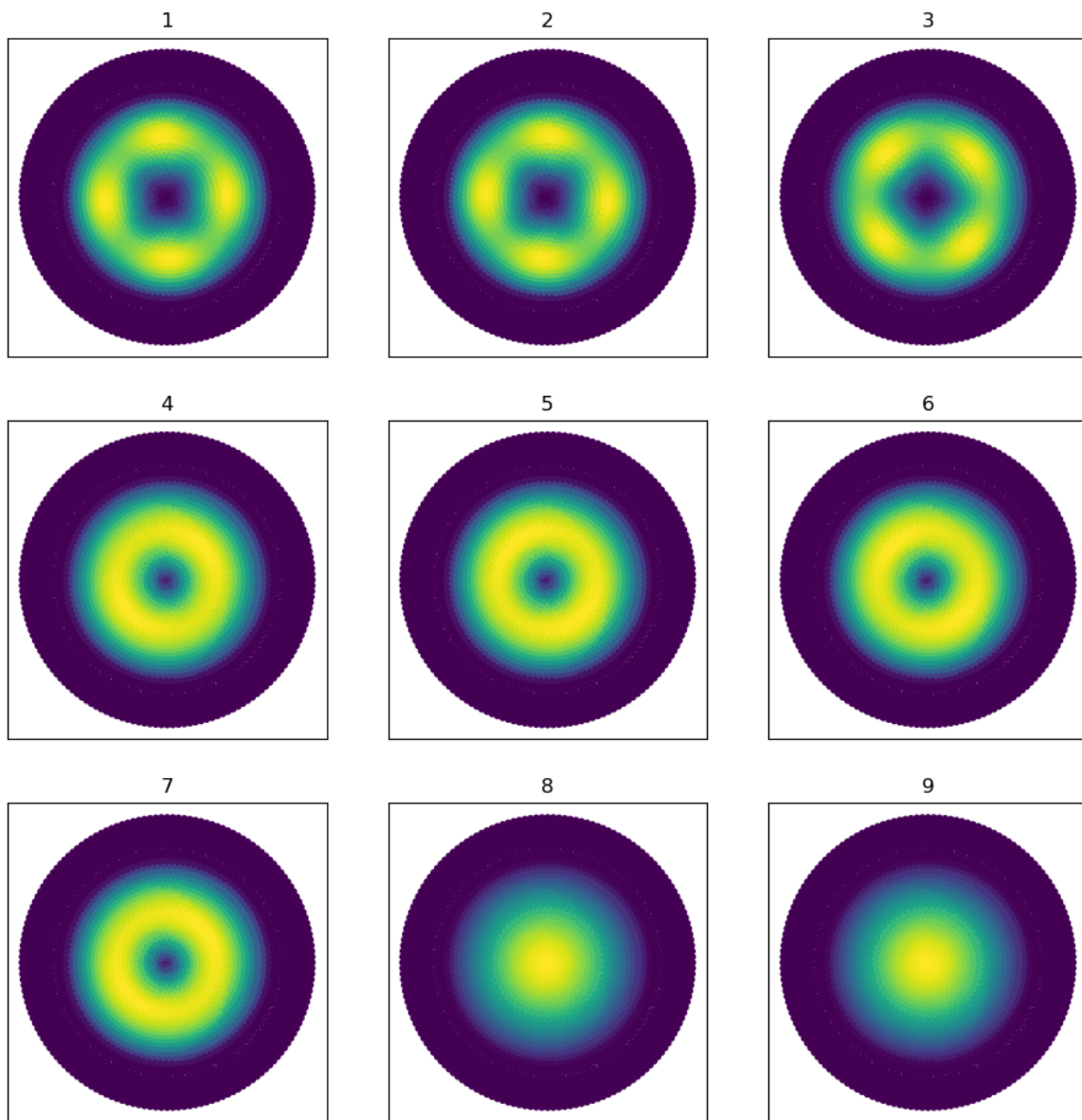
A.3. Step-index fiber Comsol

Figure A.6: Results from Comsol simulation of the norm of the electric field in V/m for the first 9 modes of Fiber B from Table 4.1, plotted with Python[14].
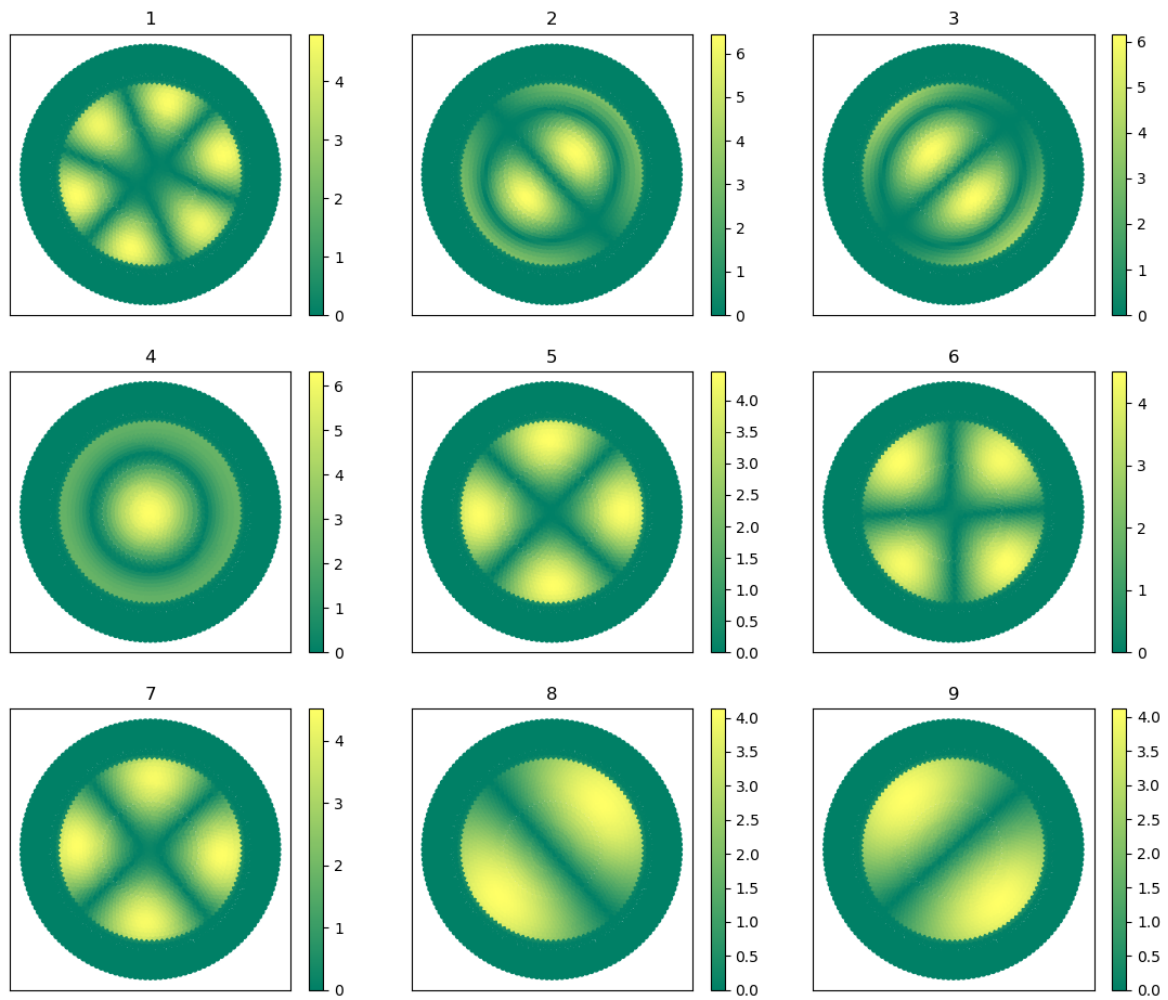
Figure A.7: Results from Comsol simulation of absolute value of the electric field in the propagation direction E_z in V/m for the first 9 modes of Fiber B from Table 4.1, plotted with Python[14].
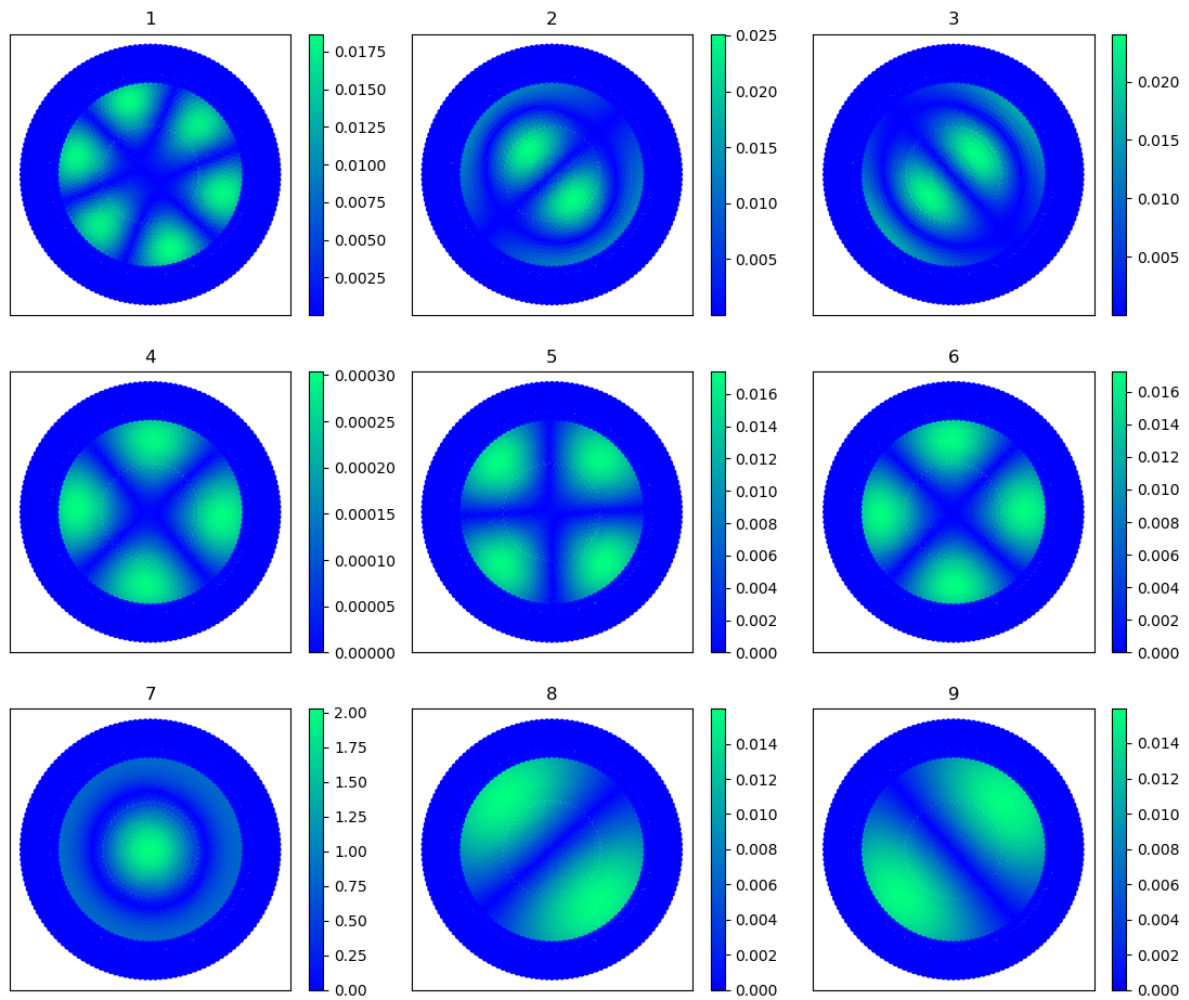
Figure A.8: Results from Comsol simulation of absolute value of the magnetic field in the propagation direction H_z in A/m for the first 9 modes of Fiber B from Table 4.1, plotted with Python[14].

Bibliography

[1]   J. Broeng et al. "Waveguidance by the photonicbandgap effect in optical fibres". In: *Journal of Optics A: Pure and Applied Optics* 1.4 (1999). URL: `https://iopscience.iop.org/article/10.1088/1464-4258/1/4/311/meta?casa_token=vjci8ImoW3QAAAAA:_K1QouAxXTdg9HGFHN5My6FBdQmt6-ZJokOhsbAZAWv8CiZd_8zzdOe-dsraAYx3aELS_PLbAw.`

[2]   A.H. Cherin. *An Introduction to Optical Fibers*. McGraw-Hill Book Company, 1982. ISBN: 978-0070107038.

[3]   W.C. Chew. *Lectures on Theory of Microwave and Optical Waveguides*. McGraw-Hill Book Company, 2021. URL: `https://arxiv.org/pdf/2107.09672.pdf.`

[4]   R.K. Chourasia and V. Singh. "Estimation of photonic band gap in the hollow core cylindrical multilayer structure". In: *Superlattices and Microstructures* 116 (Feb. 2018), pp. 191–199. URL: `https://www.sciencedirect.com/science/article/pii/S0749603618301745?via%5C%3Dihub.`

[5]   J. F. Cochran and B. Heinrich. *Applications of Maxwell's Equations*. Libre Texts, 2021. ISBN: 978-0-12-525096-2.

[6]   COMSOL. *COMSOL Multiphysics®*. Version 5.6. URL: `https://www.comsol.com.`

[7]   N. J. Cronin. *Microwave and Optical Waveguides*. Institute of Physics Publishing, 1995. ISBN: 0-7503-0216-X.

[8]   I. Dincer. "Green methods for hydrogen production". In: *International Journal of Hydrogen Energy* 37 (2 2012), pp. 1954–1971. ISSN: 0360-3199. DOI: `10.1016/j.ijhydene.2011.03.173.` URL: `https://www.sciencedirect.com/science/article/pii/S0360319911019823.`

[9]   W. C. Elmore and M. A. Heald. *Physics of Waves*. Origional work published in 1969 by Mc Graw-Hill Book Company. New York: Dover Publications, Inc., 2018. ISBN: 978-0-486-64926-9.

[10] T.J. Esselink. *Highly sensitive gas sensor in hollow-core photonic bandgap fiber: A combined experimental and numerical study*. Master Thesis. 2022.

[11] D.J. Griffiths. *Introduction to Electrodynamics*. Fourth. Cambridge University Press, 2017. ISBN: 978-1-108-42041-9. DOI: `10.1017/971108420419.`

[12] *HC-1550-02 Hollow Core Photonic Crystal Fiber*. Sold by Thorlabs. URL: `https://www.thorlabs.com/thorproduct.cfm?partnumber=HC-1550-02.`

[13] J. Hodgkinson and R. Tatam. "Optical gas sensing: a review". In: *Measurement Sience and Technology* 24 (2013). URL: `https://iopscience.iop.org/article/10.1088/0957-0233/24/1/012004/meta?casa_token=DtQli0wlEOwAAAAA:WoYfvxrk0Jf6wL37jg%5C%5C%2052icauVwmgGx3cw5okeH5kdAUWdaTfuP3iMu_R43M_WzJ5hxR3sivfdw#back-to-top-target.`

[14] Spyder IDE. *The Scientific PYthon Development EnviRonment*. Version 3.2.8. URL: `https://www.spyder-ide.org.`

[15] E. Jensen. *Cavity basics*. URL: `https://arxiv.org/pdf/1201.3202.pdf.`

[16] W. Jin et al. "Ultra-sensitive all-fibre photothermal spectroscopy with large dynamic range". In: *Nature Communications* 6.6767 (Apr. 2015). ISSN: 20411723. DOI: `10.1038/ncomms7767.`

[17] S. John. "Strong Localization of Photons in Certain Disordered Dielectric Superlattices". In: *Physical Review Letter* 58.23 (1978), pp. 2486–2489. DOI: `10.1103/PhysRevLett.58.2486.`

[18] A.P. Konijnenberg, A.J.L. Adam, and H.P. Urbach. *BSc Optics*. TU Delft Open, 2021. ISBN: 978-94-6366-396-0.

[19] B. G. Korenev. *Bessel Functions and their Applications*. London: Taylor and Francis, 2002. ISBN: 0-415-28130-x.

[20] M.G. Larson and F. Bengzon. *The Finite Element Method: Theory, Implementation and Applications*. Springer-Verlag, 2013. ISBN: 978-3-642-33287-6. DOI: `10.1007/978-3-642-33287-6`.

[21] J. Li et al. "Structure design and application of hollow core microstructured optical fiber gas sensor: A review". In: *Optics and Laser Technology* 135 (Mar. 2021). DOI: `10.1016/j.optlastec.2020.106658`.

[22] K. Mazloomi and C. Gomes. "Hydrogen as an energy carrier: Prospects and challenges". In: *Renewable and Sustainable Energy Reviews* 16 (5 2012), pp. 3024–3033. ISSN: 1364-0321. DOI: `10.1016/j.rser.2012.02.028`. URL: `https://www.sciencedirect.com/science/article/pii/S1364032112001220`.

[23] COMSOL Multiphysics. *Multiphysics Cyclopedia. The Finite Element Method (FEM)*. Mar. 2016. URL: `https://www.comsol.com/multiphysics/finite-element-method`.

[24] COMSOL Multiphysics. *Perfectly Matched Layers (PMLs)*. URL: `https://doc.comsol.com/5.5/doc/com.comsol.help.aco/aco_ug_pressure.05.106.html` (visited on 02/07/2022).

[25] COMSOL Multiphysics. *Wave Optics Module User's Guide*. 2018. URL: `https://doc.comsol.com/5.4/doc/com.comsol.help.woptics/WaveOpticsModuleUsersGuide.pdf`.

[26] K. Okamoto. *Fundamentals of Optical Waveguides*. Second. Elsevier Inc., 206. ISBN: 978-0-12-525096-2.

[27] M.N. Petrovich et al. "Robustly single mode hollow core photonic bandgap fiber". In: *Optics Express* 16.6 (Mar. 2008), pp. 4337–4346. URL: `https://opg.optica.org/oe/fulltext.cfm?uri=oe-16-6-4337&id=154938`.

[28] NKT Photonics. "HC-1550-02 Hollow Core Photonic Bandgap Fiber". In: (). URL: `https://www.newport.com.cn/medias/sys_master/images/images/he1/hc5/8797092347934/FAIR-11-1550-Data-Sheet.pdf`.

[29] "REGULATION (EU) 2021/1119 OF THE EUROPEAN PARLIAMENT AND OF THE COUNCIL". In: *Official Journal of the European Union* (June 2021). URL: `https://eur-lex.europa.eu/legal-content/EN/TXT/HTML/?uri=CELEX:32021R1119&from=EN#d1e1472-1-1`.

[30] K. Saitoh and M. Koshiba. "Leakage loss and group velocity dispersion in air-core photonic bandgap fibers". In: *Optics Express* 11.23 (Nov. 2003), pp. 3100–3109. DOI: `10.1364/oe.11.003100`. URL: `https://opg.optica.org/oe/fulltext.cfm?uri=oe-11-23-3100&id=77932`.

[31] B. Wan et al. "Characteristic Analysis and Structural Design of Hollow-CorePhotonic Crystal Fibers with Band Gap Cladding Structures". In: *Sensors* 21.1 (Jan. 2021), p. 284. DOI: `10.3390/s21010284`. URL: `https://www.mdpi.com/1424-8220/21/1/284/htm`.

[32] R. Wolfson. *Essential University Physics*. Third. Vol. 2. Pearson Education, 2016. ISBN: 978-1-292-10276-4.

[33] E. Yablonovitch. "Inhibited Spontaneous Emission in Solid-State Physics and Electronics". In: *Physical Review Letter* 58.20 (1978), pp. 2058–2062. DOI: `10.1103/PhysRevLett.58.2059`.

[34] M. Zeisberger, A. Tuniz, and M.A. Schmidt. "Analytic model for the complex effective indexdispersion of metamaterial-cladding large-areahollow core fibers". In: *Optics Express* 24.18 (2016), pp. 20515–20528. DOI: `10.1364/OE.24.020515`.